Study on the operation and energy demand of dual-stage Metal Hydride Hydrogen Compressors under effective thermal management

Gkanas, E., Stamatakis, E., Christodoulou, C., Tzamalis, G., Karagiorgis, G., Chroneos, A., Kuganathan, N., Khzouz, M. & Stubos, A. K.

Original citation & hyperlink:
Gkanas, E, Stamatakis, E, Christodoulou, C, Tzamalis, G, Karagiorgis, G, Chroneos, A, Kuganathan, N, Khzouz, M & Stubos, AK 2021, 'Study on the operation and energy demand of dual-stage Metal Hydride Hydrogen Compressors under effective thermal management', International Journal of Hydrogen Energy, vol. 46, no. 57, pp. 29272-29287.
https://dx.doi.org/10.1016/j.ijhydene.2021.02.062

DOI 10.1016/j.ijhydene.2021.02.062
ISSN 0360-3199

Publisher: Elsevier

Study on the Operation and Energy Demand of Dual-Stage Metal Hydride Hydrogen Compressors under Effective Thermal Management

Evangelos I. Gkanas[1,3*], Emmanuel Stamatakis[2,6], Christodoulos N. Christodoulou[2,5], George Tzamalis[3,7], George Karagiorgis[2,5], Alexander Chroneos[4], Navaratnarajah Kuganathan[4], Martin Khzouz[1], Athanasios K. Stubos[2,3]

[1]Centre for Advanced Low Carbon Propulsion Systems (C-ALPS), Institute for Future Transport and Cities, Coventry University, Coventry, Priory Street, CV1 5FB, UK
[2] CYRUS P.C., Lefkippos campus, 15341, Agia Paraskevi, Attica, Greece
[3]National Centre for Scientific Research Demokritos, 15341, Agia Paraskevi, Attica, Greece
[4]Faculty of Engineering, Environment & Computing, Coventry University, Priory Street, Coventry CV15FB, UK
[5]Frederick University, 7 Y. Frederickou Str., Pallouriotissa, 1036 Nicosia, Cyprus
[6]Institute of Petroleum Research / Foundation for Research and Technology - Hellas (IPR/FORTH), University Campus, Akrotiri Chania 73100, Greece
[7]Hystore Tech Ltd, Spyrou Kyprianou 30, 2643 Nicosia, Cyprus

[*]Corresponding author: ac1029@coventry.ac.uk / egkanas@gmail.com

Abstract

For the commercial viability of a hydrogen-based transportation, hydrogen infrastructure is key. One of the major issues of hydrogen infrastructure is related to the deployment and costs of the Hydrogen Refuelling Stations (HRSs), where up to 40% of the cost is related to hydrogen compression. The introduction of Metal Hydride Hydrogen Compressors (MHHCs) in the HRSs as compression elements is a potential technology to reduce operational costs, ensure noiseless operation and increase efficiency, if renewable-based thermal energy (and/or industrial waste heat) is supplied to the system. In this work, four different two-stage MHHCs are introduced and examined in terms of compression ratio, hydrogen flow rate (compression duration), thermal energy requirements and efficiency. In addition, for comparison purposes, a three-stage MHHC is also studied. The properties of five different materials are used for the individual compression stages of the MHHCs, where all the necessary thermodynamic properties are extracted experimentally and incorporated in a commercial Multiphysics software. The unsteady heat and mass transfer equations are employed for the development of the numerical model. The hydrogenation/dehydrogenation kinetics and the temperature profile were validated against solid experimental results. In addition, to improve and accelerate the storage/release kinetics, an internal thermal management scenario has been introduced. The results show that for compression at the temperature range of 10-90°C, the most favourable two-stage compression case (Case 3) showed a compression ratio of 11.18÷1, an isentropic efficiency of 4.54% with a thermal energy demand of 322 kJ/molH_2 and a cycle time of almost 34 min.

Keywords: Metal hydride hydrogen compressor; Multi-stage compression; Hydrogen storage, Metal Hydrides, Numerical Analysis

1. Introduction

The total global energy consumption related to the transportation sector in 2015 was 110 million TJ, which is equivalent to 37kWh per person on a daily basis [1-3]. At the same time, the transportation sector contributed around 29% of the total CO_2 emissions in USA [4] and 26% in EU for the year 2016 [5]. The adoption of hydrogen as an energy carrier could play a significant role in the low-carbon future of transportation [6, 7]. The use of Fuel Cell Electric Vehicles (FCEVs) that utilise an electric propulsion system based on Hydrogen Fuel Cells (HFCs) is a very effective and promising way to reduce the carbon emissions, as the only by-product of their operation is water [8-11]. One of the major obstacles for the full implementation of the FCEVs in the current low-carbon transportation market is the lack of hydrogen refuelling infrastructure (Hydrogen Refuelling Stations-HRSs) and the high cost of the existing ones, based on conventional hydrogen compressors [12, 13].

In general, a conventional HRS consists of a hydrogen production source with purification, a compression system, storage, safety and dispensation [14, 15]. Within a typical HRS, the compression of hydrogen is typically achieved by conventional mechanical-based compression [16]. According to techno-economic based research, it has been reported that these mechanical-based compressors contribute up to 40% of the total cost of the HRS [17].

An alternative way to design and develop a hydrogen compression system is by using a thermally-driven compressor based on metal hydrides. In that case, metal hydrides, with specific thermodynamic properties are connected in series and a multi-stage system is created. Based on the thermodynamic properties of those materials, the hydrogen pressure at each stage increases, and at the final stage, the pressurised hydrogen is stored in a high pressure tank [18-20]. This process of utilising metal hydrides that are able to store/release hydrogen has the potential to be an efficient way to compress pure hydrogen, as it is based on purely thermally-driven reactions for hydrogen uptake and release. MHHC's are heat engines operating in a narrow temperature range (in several cases $\Delta T=60\text{-}80^{o}C$) and, therefore, having a low efficiency limited by the Carnot one [21, 22]. Besides the purpose of compressing hydrogen, a promising field of the thermally driven hydrogen compressors is the process of hydrogen liquefaction [23, 24]. The major advantages of this technology as compared to the conventional compressors are operation simplicity, the low maintenance / operational costs, the absence of moving mechanical parts, silent operation, reliability and compactness [25, 26]. As the hydride-based hydrogen compressor depends on thermally-driven reactions of hydrogen uptake (exothermic) and hydrogen release (endothermic), it is important to note that the efficiency can be increased when solar energy or waste thermal energy from industrial sources is utilised instead of electricity [27]. Although there have been several successful attempts to integrate metal hydride-based compressors in HRSs [28], for the commercialisation and public acceptance of the hydride based hydrogen compressors, there are still several challenges to address. In a review study by Lototskyy *et al.* [29], the necessity for the development of novel materials and thermal management protocols to increase the efficiency of the compressor is highlighted. Some of the most common requirements of the materials to be employed in a MHHC are the sufficiently large reversible hydrogen storage capacity, in order to use the minimum possible quantity of materials, the tuneable P-c-T properties that will allow operation under non-extreme conditions of temperature and pressure, as well as a relatively smooth plateau slope and low hysteresis [30, 31].

The recent-developed MHHCs can be complex systems; including and integrating metal hydride beds, the connection pipes, valves, the heating and cooling systems and the passive surfaces, such as the walls and heat transfer surfaces [32, 33]. For multi-stage compressors, the properties of the materials of each stage are affecting the performance of the compressor in terms of compression ratio, the time duration of compression cycles, the efficiency and the energy needs [34-36]. A common type of materials selected for the first stage of compression are those based on the AB_5 stoichiometry, as for instance $LaNi_5$-based intermetallics that have been extensively studied in terms of storage capacity and life cycling properties [37, 38]. The research in such materials is focused mostly on the partial substitution of La with Ce and of the Ni-part with other transition metals, such as Co, Al and Sn, in order to change the thermodynamic properties of the materials and enhance their stability, as well as to reduce the degradation during cycling [39, 40]. On the other hand, the substitution with various elements could affect the plateau slope and the hysteresis of the materials [41, 42]. For the later stages of the compression system, intermetallics with the AB_2 stoichiometry have been studied, mainly based on the combination of the following elements: Zr-Ti-Fe-Cr-V [43-46]. The AB_2-intermetallics with industrial importance crystallise on either the hexagonal C14 ($MgZn_2$) and C36 ($MgNi_2$) or cubic, C15 ($MgCu_2$) Laves phases [47, 48]. In addition, besides the complexity of such systems, a large scale commercial system needs to consider the material(s), the connections, the geometry and the thermal management of the reactors to accelerate the compression process [49]. All the above parameters may increase the total cost of the product. Thus, the development of numerical models that will be able to successfully simulate and predict the compression process and at the same time to identify effective heat management scenarios is crucial and of great importance.

Several studies regarding the numerical description of the hydrogenation / dehydrogenation process during the hydrogen compression process have been released, based on the coupled heat and mass transfer [50-58]. More specifically, a hybrid model describing the free volume of the reaction vessel for a dual-stage compression system has been introduced [59]. The model designed to numerically describe large-scale industrial compressors that contain several reactors operating in a non-synchronous manner. In another study, unsteady heat and mass transfer equations have been introduced involving the desorbing and the absorbing reactors during the coupling process to simulate a three-stage compressor [60].

Other researchers have considered the implementation of several H_2 equations of state combined with realistic features for the hydrogen sorption properties [61]. The implementation of real/ideal gas models and their effect on the P-c-T isotherms was highlighted. More recently [62], an approach to simulate the performance of a seven-stage metal hydride-based compressor has been presented. Several parameters have been studied, such as the compression ratio, the compression duration and the thermal energy requirements of the system. The numerical model was based on the introduction of the unsteady heat and mass conservation equations for the description of a device based on seven novel materials that have been specifically synthesised, characterised and tested for hydrogen compression purposes.

In the current work, a numerical approach to describe and compare the operation of various two-stage MHHC systems is introduced and analysed. For comparison purposes, a three stage system is also studied. The analysis is focusing on evaluating the operation of the studied compressors in terms of compression ratio, thermal energy requirements per compression cycle and compression efficiency. Five cases of compression systems are considered. The first four cases relate to two-stage systems and the final case concerns the development of a three-stage system. For all the five different materials employed in the compression processes, the parameters utilised, such as the effective thermal conductivity of each material, the plateau slope and the hysteresis, the specific heat capacity and the hydrogenation/dehydrogenation characteristics have been extracted by experimental results and presented in the manuscript. The kinetics for both the hydrogenation and dehydrogenation of all the studied materials have been validated against solid experimental data. The main differences and novelties of the current study, as compared to some previous studies from the authors and other research groups, relate to the introduction of an extended numerical model and analysis (accounting also for the cooling / heating fluid flow in the heat exchangers) that simulates and evaluates the thermal management scheme, whereas, in most studied cases, only an external heating / cooling jacket is normally considered. In addition, this study considers a large-scale approximation, where the length of each metal hydride tank reaches 9.2 m, allowing to test more than 50 kg of material and assess the heat transfer designs and associated effects along the tank (in connection to e.g. fluid flow rates, various design and geometry features, etc.), whereas the majority of studies (including studies by the present authors) consider relatively small, lab-scale compressors with simple, fixed heat management characteristics. Finally, the AB_2-based materials used in the current study have been developed specifically for the current application and present some very interesting properties for the development of a two-stage MHHC, while the main properties and the isotherms measured experimentally are also presented in the study.

2. Model Formulation

A complete two-stage compression cycle consists of an initial hydrogenation process, followed by a coupling (dehydrogenation - hydrogenation) between the two stages and the dehydrogenation of the final stage to the storage tank. At the beginning of the compression, the temperature of stage 1 is low (in this study 10 ^oC) and hydrogen is introduced in the vessel at low pressure from a hydrogen supplier, such an electrolyser. During the hydrogenation process at stage 1, the temperature of the reactor increases as per the exothermic nature of the reaction. After the maximum amount of hydrogen stored at stage 1, a sensible heating of the vessel takes place. As per the van’t Hoff law, the pressure will increase at stage 1. After that point, the coupling between stage 1 (dehydrogenation) and stage 2 (hydrogenation) takes place. Finally, a sensible heating of the stage 2 follows, leading to the dehydrogenation process of stage 2. The compression process is a thermally driven process; thus, the selection of the materials for the compression stages should be based on strict criteria of pressure and thermal requirements.

2.1 Numerical Model

For the development of a numerical description for a process that includes chemical reactions, diffusion in porous media, heat transfer and coupling between different systems, the introduction of several assumptions is necessary. For the establishment of the present numerical model the following assumptions have been considered:

i. At the beginning of the hydrogenation and the dehydrogenation processes, the temperature and pressure profiles within the system (each reactor) are uniform.
ii. The material within each reactor (stage) is in local thermal equilibrium that implies no heat transfer between the gas and the solid phase.
iii. The characteristics (kinetic and thermal) of the materials are assumed unaffected from the cycling (no degradation over cycling).
iv. Perfect packing conditions between the metal hydride powder and the reactor.
v. Radiative heat transfer and viscous dissipation are negligible.

2.2 Energy Equation for Metal Hydride

By considering the local equilibrium between the solid and the gas phase (equal gas and solid phase temperature within the metal hydride vessel), a single energy equation is introduced:

$$\begin{aligned}&(\rho \cdot Cp)_e \cdot \frac{\partial T}{\partial t} + (\rho_g \cdot Cp_g) \cdot \bar{v}_g \cdot \nabla T \\ &= \nabla \cdot (k_e \cdot \nabla T) + \dot{m} \cdot (\Delta \mathrm{H} - T \cdot (Cp_g - Cp_s))\end{aligned} \tag{1}$$

In Eq (1), the term $(\Delta H - T \cdot (Cp_g - Cp_S))$ represents the heat source term (W/m^3). The parameter $\dot{m}$ *(kg/m^{3}s)* represents the kinetics for the hydrogenation and dehydrogenation and will be analysed in 2.4. In addition, Cp_g and Cp_s is the specific heat capacity (J/kg/K) for the gas phase (hydrogen) and the solid phase (hydride) respectively. The terms ρ_g and v_g represent the hydrogen density (kg/m^3) and velocity (m/s). Finally, ΔH (J/molH$_2$) is the enthalpy change during the hydrogenation/dehydrogenation.

The term $(\rho \cdot C_P)_e$ considers the effective heat capacity that takes into account the contribution of both the hydride and the hydrogen gas within the reactor and is updated by:

$$(\rho \cdot Cp)_e = (\varepsilon \cdot \rho_g \cdot Cp_g \ ) + ((1-\varepsilon) \cdot \rho_s \cdot Cp_s) \tag{2}$$

The effective thermal conductivity is estimated by utilising the Zehner, Bauer and Schlunder method that calculates the thermal conductivity within packed beds [63]:

$$k_{eff} = \frac{C_1 \cdot p^{C_2}}{\frac{1}{C_0} + p^{C_2}} \tag{3}$$

In Eq. 3, C_o, C_1 and C_2 are fitting coefficients [64].

2.3 Hydrogen and Solid (metal/hydride) Mass and Momentum Conservation

For the hydrogen gas, the mass conservation within the metal hydride vessel is expressed by the continuity equation:

$$\varepsilon \cdot \frac{\partial(\rho_g)}{\partial t} + div(\rho_g \cdot \vec{v}_g) = -\dot{m} \tag{4}$$

For the metal hydride (solid phase), the continuity equation is given by:

$$(1-\varepsilon) \cdot \frac{\partial \rho_{solid}}{\partial t} = \dot{m} \tag{5}$$

By introducing the compressibility factor *Z(p,T)* representing the deviation of the real gas behaviour from the ideal behaviour, the density of hydrogen is given by:

$$\rho_g = \frac{p \cdot M_g}{Z(\mathrm{p},\mathrm{T}) \cdot R \cdot T} \tag{6}$$

The gas velocity through the porous medium can be described by Darcy's law, which describes the flow of a fluid in a porous medium. By neglecting the gravitational effect, the relationship between the flow rate and the pressure drop is given by:

$$\vec{v} = -\frac{k}{\mu} \cdot \nabla p \tag{7}$$

In Eq. 7, K (m^2) is the permeability of the material and μ represents the dynamic viscosity of the hydrogen gas. The permeability is given by Eq. (8) (Kozeny–Carman's equation):

$$K = \frac{dp^2 \cdot \varepsilon^3}{180 \cdot (1-\varepsilon^2)} \tag{8}$$

2.4 Heat Exchanger Energy Equation and Heat Exchanger Walls

The flow of the cooling/heating fluid in the heat exchanger is described by the Navier-Stokes equation:

$$\frac{\partial V_f}{\partial t} + (\rho_f \cdot \vec{V}_f \cdot \nabla\vec{V}_f) = \nabla \cdot \left[n_f \left(\nabla\vec{V}_f + \left(\nabla\vec{V}_f\right)^T\right)\right] - \nabla p_f \tag{9}$$

The energy equation used within the fluid domain is Equation 10:

$$\rho_f C p_f \frac{\partial T_f}{\partial t} + \nabla\left(\rho_f \vec{V}_f T_f\right) = \nabla \cdot (k \nabla T_f) \tag{10}$$

Where, V_f $(m\ s^{-1})$ is the fluid velocity, T_f(K) is the fluid temperature, Cp_f $(J\ kg^{-1}\ K^{-1})$ represents the fluid specific capacity and ρ_f $(kg\ m^{-3})$ is the fluid density.

The boundary condition used at the heat exchanger walls is:

$$-\hat{n} \cdot q = h_e(T - T_f) \tag{11}$$

Where h_e $(W\ m^{-2}\ K^{-1})$ is the effective heat transfer coefficient. The effective heat transfer coefficient in this work is updated by the following [65]:

At the laminar flow regime (for Reynolds numbers Re<2300) h_e is updated by:

$$h_e = \frac{k_f}{D_{tube}}\left[5.4 + \frac{0.0019\left(\frac{Re \cdot Pr \cdot D_{tube}}{L}\right)^{1.71}}{1+0.00563\left(\frac{Re \cdot Pr \cdot D_{tube}}{L}\right)^{1.71}}\right] \tag{12}$$

At the transition flow regime (2300<Re<6000)

$$h_e = \frac{k_f}{D_{tube}}\ 0.166(Re^{0.67} - 125){P_r}^{0.33}\left[1 + \left(\frac{D_{tube}}{L}\right)^{0.67}\right]\left(\frac{\mu_f}{\mu_{fw}}\right)^{0.14} \tag{13}$$

At the turbulent flow regime (Re>6000)

$$h_e = \frac{k_f}{D_{tube}}\ 0.018 Re^{0.8} {P_r}^{0.4} \tag{14}$$

In Equations 12-14, P_r is the Prandtl Number, D_{tube} (m) is the diameter of the heat exchanger tube, L (m) is the length of the helical heat exchanger, k_f (W $m^{-1}K^{-1}$) is the thermal conductivity of the fluid, μ_f and μ_{fw} $(Pa\ s)$ are the fluid viscosity values as calculated at the fluid temperature and the at the wall temperature respectively.

2.5 Hydrogenation/Dehydrogenation Kinetic Terms

The rate for the hydrogenation and dehydrogenation process is updated from the following equations:

For the hydrogenation process:

$$\dot{m}_{abs} = C_{abs} \cdot e^{\left(\frac{-E_{abs}}{R \cdot T}\right)} \cdot ln\left(\frac{P}{P_{eq}}\right) \cdot \delta\rho \tag{15}$$

For the dehydrogenation process:

$$\dot{m}_{des} = C_{des} \cdot e^{\left(\frac{-E_{des}}{R \cdot T}\right)} \cdot \left(\frac{P_{eq} - P}{P_{eq}}\right) \cdot \delta\rho \tag{16}$$

In Eq. 15 and 16, C_{abs} $[s^{-1}]$ and C_{des} $[s^{-1}]$ are pro-exponential constants for absorption and desorption respectively, E_{abs} $[J/mol]$ and E_d $[J/mol]$ represent the activation energy for the hydrogenation/dehydrogenation processes respectively and $\delta\rho$ $[kg/m^3]$ is the density difference between the saturation density of the hydride and the density at any time during the reaction.

2.6 Equilibrium Pressure for the Hydrogenation/Dehydrogenation

In the present study, the equilibrium pressure is provided by the modified van't Hoff equation, when the plateau and hysteresis are introduced [66, 67]:

$$\ln P_{eq} = [\frac{\Delta \mathrm{H}}{R_g \cdot T} - \frac{\Delta S}{R_g} + (\sigma_s \pm \sigma_0) \cdot \tan(\pi(\frac{X}{X_{\max}} - \frac{1}{2})) \pm \frac{\mathrm{Y}}{2}] \cdot P_0 \tag{17}$$

In Eq. 17, σ_s and σ_0 are the plateau flatness parameters and Y is the hysteresis. All of these parameters are measured experimentally from the isotherms for all the materials used in the current study. The incorporation of the above parameters in the equilibrium pressure is crucial, as the majority of the materials that are used for metal hydride compression purposes present a relative high slope and hysteresis. The hysteresis is represented by the following expression:

$$Hysteresis = \ln(\frac{P_A}{P_D}) \tag{18}$$

Where P_A and P_D denote the pressure for the hydrogenation and dehydrogenation respectively [5]. In addition, the plateau slope is calculated by the following expression [68]:

$$Slope = \frac{d(lnP)}{d(HM)} \tag{19}$$

The slope flatness in this work was calculated by the linear flatness analysis when the data were fitted to a least squares plane. The values for the flatness factors and the hysteresis for all the extracted materials are presented in Table 2.

2.7 Equations for the Coupling (Dehydrogenation/Hydrogenation) Process

When trying to establish a numerical model to describe the coupling process between the compression stages, the amount of hydrogen and the pressure are crucial parameters for the proper description of the system. At the same time, the remaining hydrogen that is stored in gaseous phase in the free volumes of the tanks has to be considered when calculating the pressure after the hydrogen release/storage. The two reactors are connected to each other by an interconnector, as depicted in Fig. 1. The number of hydrogen moles entering the interconnector from reactor 1 (point 1 in Fig. 1) and the hydrogen moles exiting the interconnector to be stored at reactor 2 (point 2 in Fig. 1) are critical parameters that need to be established. The number of hydrogen moles within the interconnector during the coupling is updated by:

$$n_t = n_{in} + n_{des} - n_{abs} \tag{20}$$

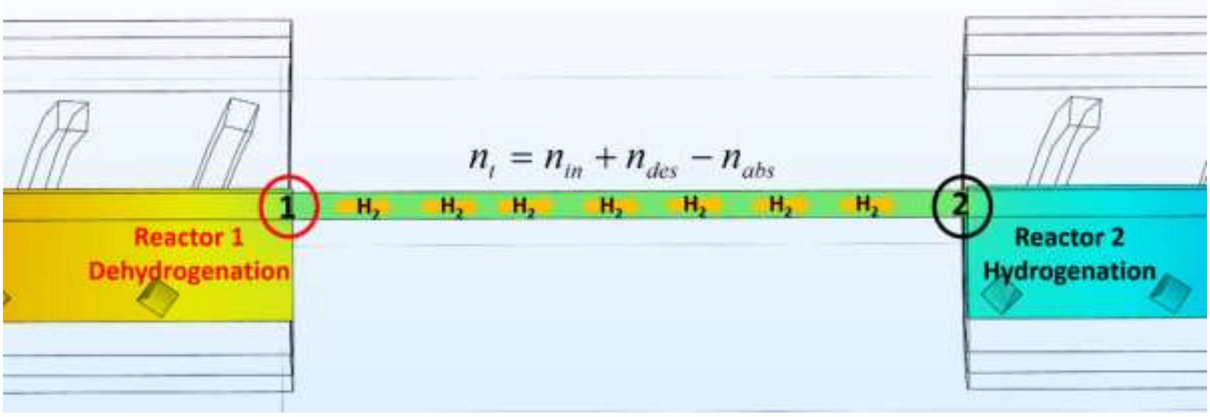

Fig. 1. Schematic of the hydrogen movement during the coupling process between the two stages

In Eq. 20, n$_{in}$ refers to the initial amount of hydrogen present in the interconnector, whereas n$_{des}$ and n$_{abs}$ refer to the amount of hydrogen stored (reactor 2) and the amount of hydrogen released from reactor 1 respectively. The pressure of the hydrogen gas in the interconnector is given by:

$$p_t = \frac{n_t \cdot R_g \cdot T}{V_1 + V_2} \tag{21}$$

In Eq. 21, the terms V_1 and V_2 (m^3) are the free volumes of each reactor (reactor 1 and 2), n_t is the amount of hydrogen moles at any time within the interconnector and T (K) is the gas temperature in the interconnector. This pressure represents the driving force for both dehydrogenation of reactor 1 and hydrogenation of reactor 2 and the kinetics for the dehydrogenation / hydrogenation during the coupling are given by the following:

For the dehydrogenation process:

$$\dot{m}_{des} = C_{des} \cdot e^{\left(\frac{-E_{des}}{R \cdot T}\right)} \cdot \left(\frac{P_{eq} - p_t}{P_{eq}}\right) \cdot \delta\rho \tag{22}$$

For the hydrogenation process:

$$\dot{m}_{abs} = C_{abs} \cdot \exp\left(\frac{-E_a}{R_g \cdot T}\right) \cdot \ln\left(\frac{p_t}{P_{eq}}\right) \cdot (\rho_{ss} - \rho_s) \tag{23}$$

3. Methodology

3.1 System and Materials

The main objective of this work is the investigation on the performance of four two-stage compressors, when 500 g H_2 are to be compressed per compression cycle. This amount is to be delivered at the output of the compressor when the compressed gas is stored at the high pressure tank. In addition, for comparison purposes, a three-stage compressor is studied. A heat management scenario is considered to enhance the hydrogenation/dehydrogenation kinetics, by introducing a coil heat exchanger in addition to the outside contribution of a co-central shell heat exchanger. More information regarding the geometry of the reactors will be given in the upcoming chapters. The proposed numerical model was incorporated in a commercial Multiphysics software (COMSOL Multiphysics 5.3). The first step is the validation of the numerical model with solid experimental data of the hydrogenation/dehydrogenation kinetics and the temperature for all the materials used. Figure 2 presents the hydrogenation/dehydrogenation isotherms that have been obtained for one of the materials used in this study (M5) at two temperatures (10 and 80 °C). The enthalpy and entropy for the hydride formation/deformation (ΔH and ΔS) have been calculated based on the experimental isotherms for all the materials. More specifically, P-c-T isotherms have been recorded for all the materials at various temperatures. Then, by introducing the data for at least three isotherms, the van't Hoff plots have been developed by using the hydrogen concentrations at the mid-plateau point. From the slope and the intersection with the y-axis we have extracted the values of enthalpy and entropy. The P-c-T isotherms for all the samples recorded at two temperatures (10 and 80°C) are presented at the supplementary data (S1). In addition, the authors must highlight that because of the high pressures that the materials (especially the M3-M4 and M5) can reach at high temperatures, the measurement of the full isotherm at such temperatures is a challenge. For that reason, for each material, various isotherms have been recorded; at relatively low temperatures (10-20-30 °C), low temperatures (5, 0 and -5 °C) and then at higher temperatures (80-90 and 100 °C) - but no higher than the levels of the pressure that were safe for the system (Sievert Apparatus). Thus, by collecting the data at various temperatures, the authors trust that the values of enthalpy and entropy taken into account in the current study are as valid as they could be.

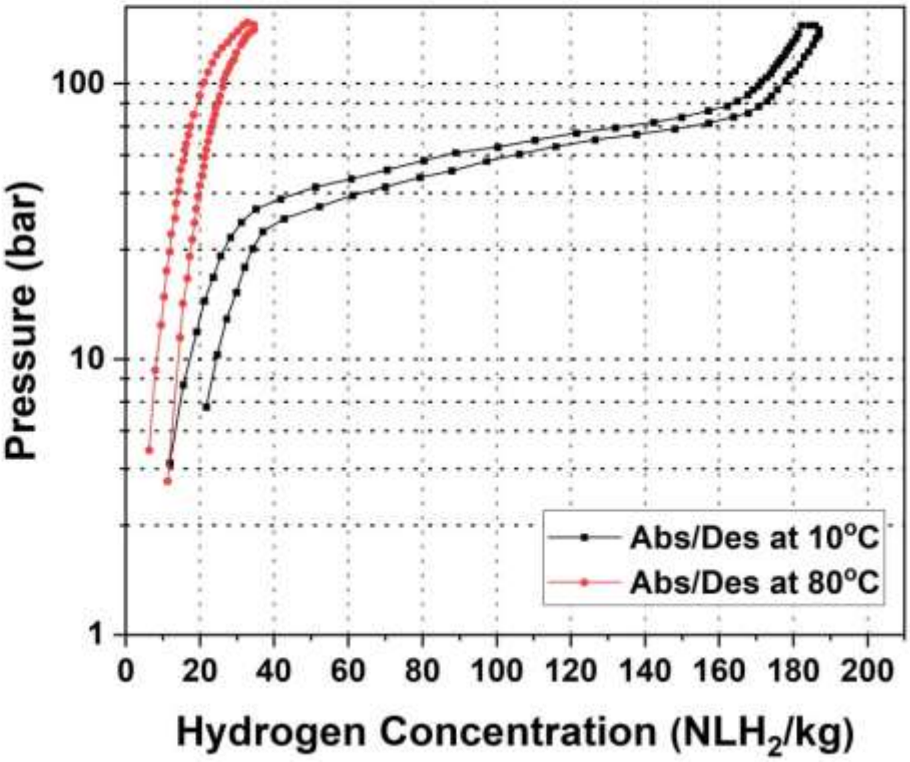

Fig. 2. PcT curves for one of the materials used in this work (M5) at two temperatures (10 and 80 °C)

The operation temperature range for the studied compressors is 10 °C (hydrogenation) and 90 °C (dehydrogenation), so water was the medium to be used as the cooling/heating fluid. Table 1 summarizes all the materials that have been synthesized, tested and used in this work.

Table 1. Summary and thermodynamic properties of the materials used in the present study

Material Name	**Type**	**ΔHabs ($J/molH_2$)**	**ΔSabs (J/molH2/K)**	**ΔHdes ($J/molH_2$)**	**ΔSdes ($J/molH_2/K$)**
M1	AB_5	-25242	-104.02	28195	106.78
M2	AB_2	-21466	-94.62	26133	107.02
M3	AB_2	-21354	-101.05	24823	109.01
M4	AB_2	-19991	-100.01	20085	100.48
M5	AB_2	-18198	-98.07	19856	101.41

More specifically, the material M1 has the stoichiometry AB_5, where A=La-Ce and B=Ni. The remaining 4 materials (*M2-M5*) are based on the AB_2 stoichiometry, where A=Ti-Zr, B=Cr-Mn-Ni-Fe-V. All the intermetallics have been synthesized by arc-melting, while their P-c-T properties were measured by a commercial Sievert-type apparatus (*Hidden Isochema*), to estimate the thermodynamic properties needed for the numerical calculations. The structural characterisation and the chemical composition of the synthesised samples, as well as the indication of the lattice expansion during the hydrogenation has been performed by X-ray diffraction along with the Rietveld refinement. The XRD spectra for the sample M1 prior and after the hydrogenation is presented in the supplementary data (Figure S2a). In addition, the Rietveld refinement to identify the composition and the phases is presented in Fig. S2b. According to those results, the material has a single-phase composition with the $CaCu_5$ hexagonal structure (space group P6/mmm [191]). In addition, from the Figure S2a, there is a shift of the peaks towards lower diffraction angles, indicating a lattice expansion (for M1 has been calculated to 29%), which is very important safety aspect for the design of metal hydride tanks (especially for those to be used at high pressures). Table 2 presents the properties of the materials that have been used for the numerical investigations.

Table 2. Properties of the materials used in the current study.

Sample	Density Bulk	Effective thermal conductivity	Flatness Factor at 10^{o}C	Hysteresis at 10^{o}C
M1	8478 kg/m^3	0.588 W/m/K	0.08	1.09
M2	6304 kg/m^3	0.298 W/m/K	0.141	0.32
M3	6448 kg/m^3	0.396 W/m/K	0.148	0.11
M4	6609 kg/m^3	0.488 W/m/K	0.169	0.21
M5	6617 kg/m^3	0.494 W/m/K	0.152	0.11

In addition, Table 3 summarizes all the compression cases considered in the current study.

Table 3. Summary of all the compression cases and conditions used in the current study

Case	No. Stages	Materials Stage 1–Stage 2	T_{abs} (°C)	T_{des} (°C)	Supply Pressure (bar)
Case 1	2	M1 - M2	10	90	20
Case 2	2	M2 – M3	10	90	20
Case 3	2	M2 – M4	10	90	20
Case 4	2	M4 - M5	10	90	50
Case 5	3	M2 – M4 – M5	10	90	20

3.2 System Geometry

The geometry of the metal hydride tanks is presented in Fig. 3. In order to compress 500 g of H_2 at the end of the compression cycle, an amount of hydrogen higher than 500 g has to be stored in the previous stage(s). The total amount of hydrogen involved during the compression cycle, including the hydrogen between the stages is expected to be more, and this involves the hydrogen that is being stored on solid state along with the hydrogen that is in gaseous form inside the beds. Thus, the amounts of the metal hydrides that will be selected for each stage of the compressor are key parameters for the development of the compressor. Thus, the amounts of the metal hydrides that will be selected for each stage of the compressor are key parameters for the development of the compressor. In addition, the calculation metal hydride masses should consider the amount of hydrogen that is stored in gaseous form in the empty space of the system. Thus, the amount of material 1 (M1) should be almost 54 kg, the amount of material 2 (M2) almost 47 kg and the amount for the rest three materials (M3-M4-M5) around 44 kg. The amounts of materials used in this study have been calculated by taking into account the effective density of the metal hydride powders and the maximum reversible hydrogen storage/release capability of each material while also taking into account the amount of the hydrogen that will be stored in gaseous phase in the empty space inside the metal hydride bed. In addition, for safety reasons, due to the expansion of the materials during cycling (26% up to 31%) the reactors were considered to be filled up to 50%. Thus; the length each reactor is 9.2 m, the internal radius is 34.2 mm, the internal wall thickness is 10 mm and the thickness of the cooling/heating shell is 8 mm, as illustrated in Fig.3a and Fig. 3b. In the centre of the tanks, a porous sintered filter is installed to introduce/remove the H_2 gas during the hydrogenation/dehydrogenation respectively. The thermal management of the tank takes place both internally and externally. The external heat management is performed via the external cooling/heating shell and the internal heat management via the spiral heat exchanger as illustrated in Fig. 3c. The external walls of the spiral heat exchanger are in contact with the internal walls of the tank (Fig. 3d).

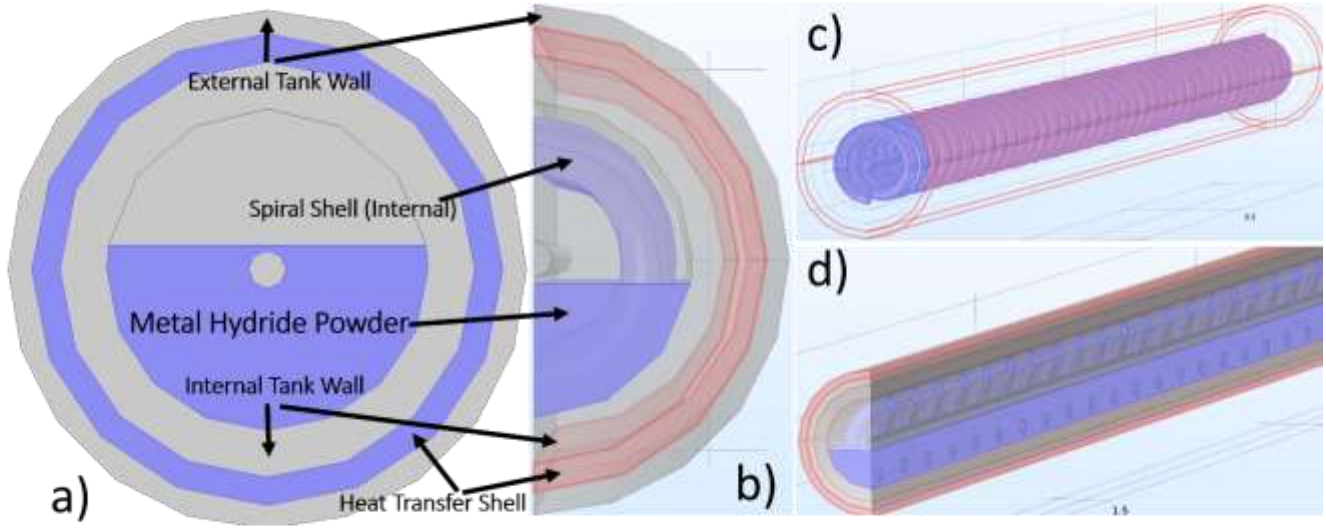

Fig. 3. Schematic of the geometry considered in this work. Fig. 3a shows the cross-section of the metal hydride tanks. Each tank consists of a porous sintered pipe to deliver and remove hydrogen to/from the bed (centre), the metal hydride material which is placed inside the bed. The thermal management takes place both internally and externally. The internal heat management takes place via a spiral heat exchanger (Fig. 3b and 3c) and a cylindrical shell is also utilised for external thermal management (Fig. 3a and 3b).

3.3 Validation of the numerical approach

The proposed numerical model has been validated against solid experimental data. The density of the materials was measured by a gas displacement pycnometry system (Micrometrics Accupycn1340). The values for the thermal conductivity were obtained by using a commercial thermal conductivity analyser (C-therm Technologies). This instrument provides the opportunity to use three different ways to measure the thermal conductivity. In our case, we have used the MTPS (Modified Transient Plane Source) method, where a heat interfacial heat reflectance sensor applies a momentary heat source to the powder. The thermal conductivity is recorded automatically. The hydrogenation/dehydrogenation data were obtained by a commercial Sievert-type apparatus (Hidden Isochema) and the isotherms obtained for M5 are presented in Fig. 2. The isotherms of each material were measured at several temperatures (at least three) to create the van’t Hoff diagram. From the van’t Hoff plots, the reaction enthalpy and entropy change (ΔH and ΔS) were obtained. Samples of almost 1g were used to measure the hydrogenation/dehydrogenation kinetics and the temperature evolution of the reactions. The kinetics presented in Fig. 4d were measured at defined hydrogen supply pressures and the initial temperature of the powder was set at 20°C. A *K*-type thermocouple was placed close to the centre of the sample in a vertical position (Fig. 4a and 4b). Fig. 4c presents the temperature profile during the hydrogenation process for the material M2. The dots represent the experimental data, whereas the straight line represents the simulation results. In addition, Fig. 4d shows the comparison between the experimental and the simulated hydrogenation kinetics for the same material (M2). The numerically predicted temperature and hydrogenation behavior are in good agreement with the experimental results.

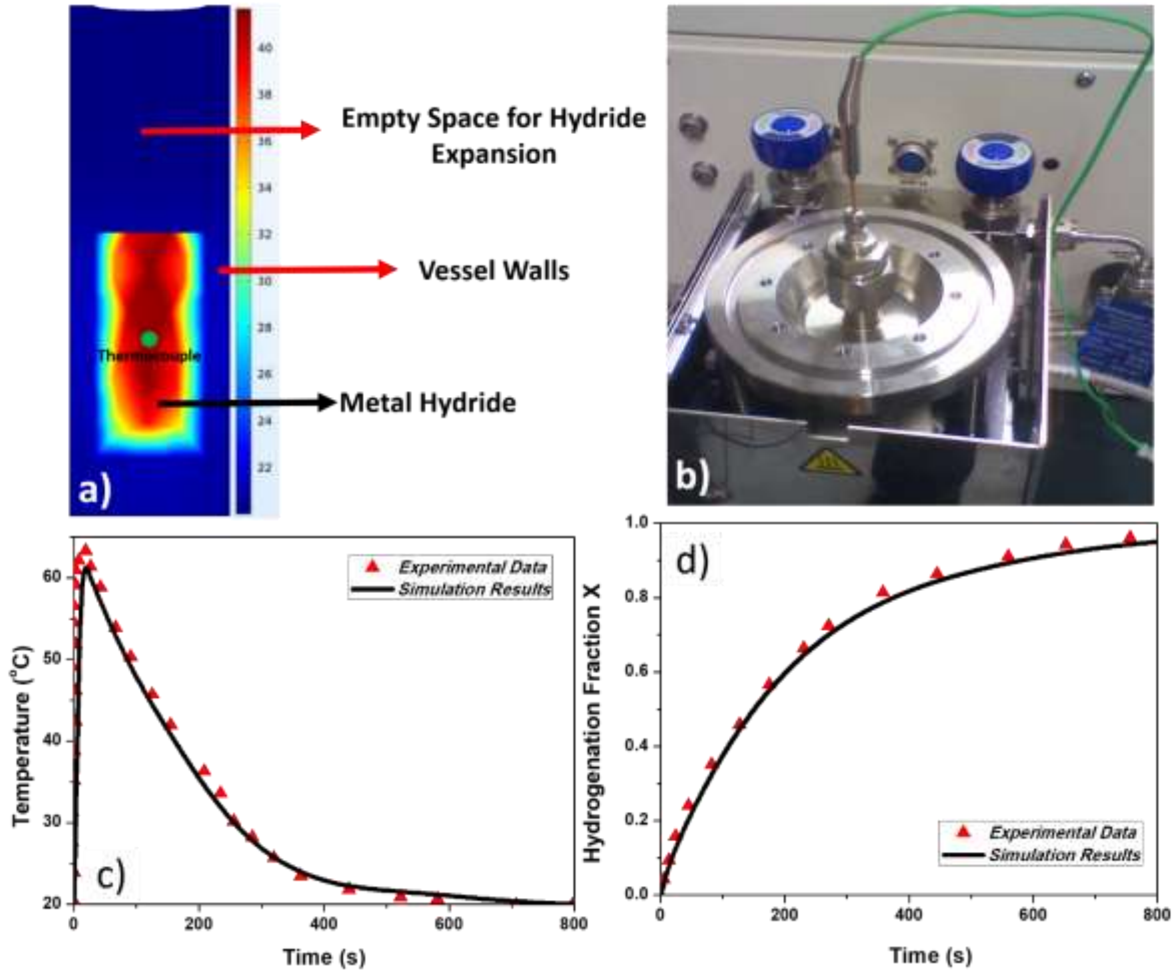

Fig. 4. Validation of the proposed numerical model with experimental results. Fig. 4a and 4b present the simulated geometry and the actual experimental geometry respectively. Fig. 4c presents the validation of the temperature profile and Fig. 4d the hydrogenation capacity for the case of material M2.

4. Results and Discussion

In the current work, four different cases of two-stage MHHC systems are studied. In addition, a three-stage compression system is considered for comparison purposes. The above systems are based on the combination of the five materials (M1-M5) that have been introduced and discussed in the previous chapter. For the two-stage systems, a complete compression cycle consists of one individual hydrogenation (stage 1) with a subsequent sensible heating. The pressure inside stage 1 system after the sensible heating is at high level and thus, when the valve between stage 1 and stage 2 opens the hydrogen from stage 1 is entering the stage 2 and is stored. After this coupling process between stage 1 and stage 2, the stage 2 system undergoes another sensible heating process. Finally, the stage 2 reactor releases hydrogen gas in a high-pressure tank. The process is exactly the same for the three-stage system; the only difference is the existence of an extra coupling between stage 2 and stage 3.

4.1 Temperature and pressure profile for the multi-stage hydrogen compression

The combination of the materials involved in the five compression systems is presented in Table 3. The temperature for the hydrogenation and the dehydrogenation processes is 10 ^{o}C and 90 ^{o}C respectively. The initial supply pressure for each system is 20 bar; similar to the pressure that a commercial electrolyser can supply. The only exception is Case 4, where the initial pressure is 50 bar, as the material M4 used at stage 1 has an equilibrium pressure of almost 35 bar at 10 ^{o}C. For the operation of the compressor, each material operates between 10% and 90% of the theoretical maximum hydrogenation/dehydrogenation capacity. The reason for that decision arises from the hydrogenation/dehydrogenation kinetic plots, where it is extracted that when the materials stores 90% of the maximum theoretical reversible storage capability, the kinetic curve reaches a plateau, where the absorption at that point takes place in a very slow rate. The same behaviour is observed during the dehydrogenation process, when the material releases the stored hydrogen down to 90% (or when 10% of H_2 left), then the kinetic curve is also reaching a plateau, and the rest of the stored hydrogen is released on a very slow pace. Thus; to accelerate the operation of the compressor the materials are operating between these ranges, as seen in Fig. 5 for the system of Case 5.

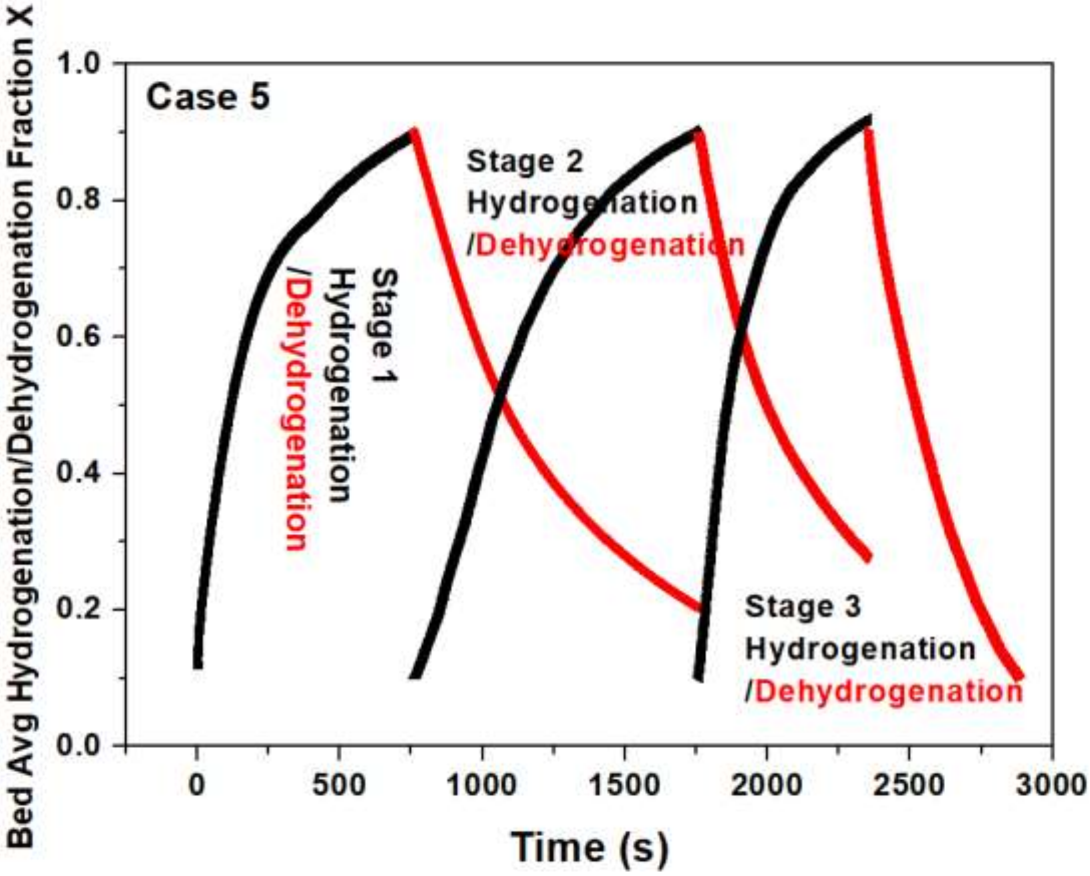

Fig. 5. Bed average hydrogenation/dehydrogenation capacity for the three-stage compression system used in the current study (case No. 5). For the effective operation of the compression system, the materials are operating between the ranges of 10-90% of their theoretical storage capacity.

The temperature evolution of the complete compression cycle for Case 5 is presented in Fig. 6. At the beginning of the hydrogenation process, hydrogen is driven into the stage 1 hydride bed. As hydrogen storage within the interstitials of the material and the development of the new phase (hydride) take place, due to the exothermic nature of the reaction, a sudden temperature rise takes place. The temperature increases during the first stage of the hydrogenation up to a maximum value that mainly depends on the hydrogen pressure and the thermal management of the system and gradually drops, as a result of the combination between the reaction kinetics and the thermal management. The temperature drop is not instantaneous but gradual, as a result of the relatively poor thermal conductivity of the metal hydride powder that doesn’t allow for the effective and fast heat removal. Especially for the compression operation, due to the high pressure during operation, for safety reasons, the wall thickness is higher as compared to a conventional tank for solid-state hydrogen storage. This is another factor that makes the thermal management in that case less efficient. For that reason, in the current work, besides the external thermal management, an internal thermal management scenario is considered. The actual sensible heating/cooling processes are not depicted realistically in Fig. 6 to keep the temperature profile simple; thus, those processes are depicted by the vertical dashed lines. In the case of the three-stage compressor there are three-sensible heating processes. The sensible heating processes are necessary to increase the pressure within each stage, in order to prepare the material for the upcoming coupling with the next stage.

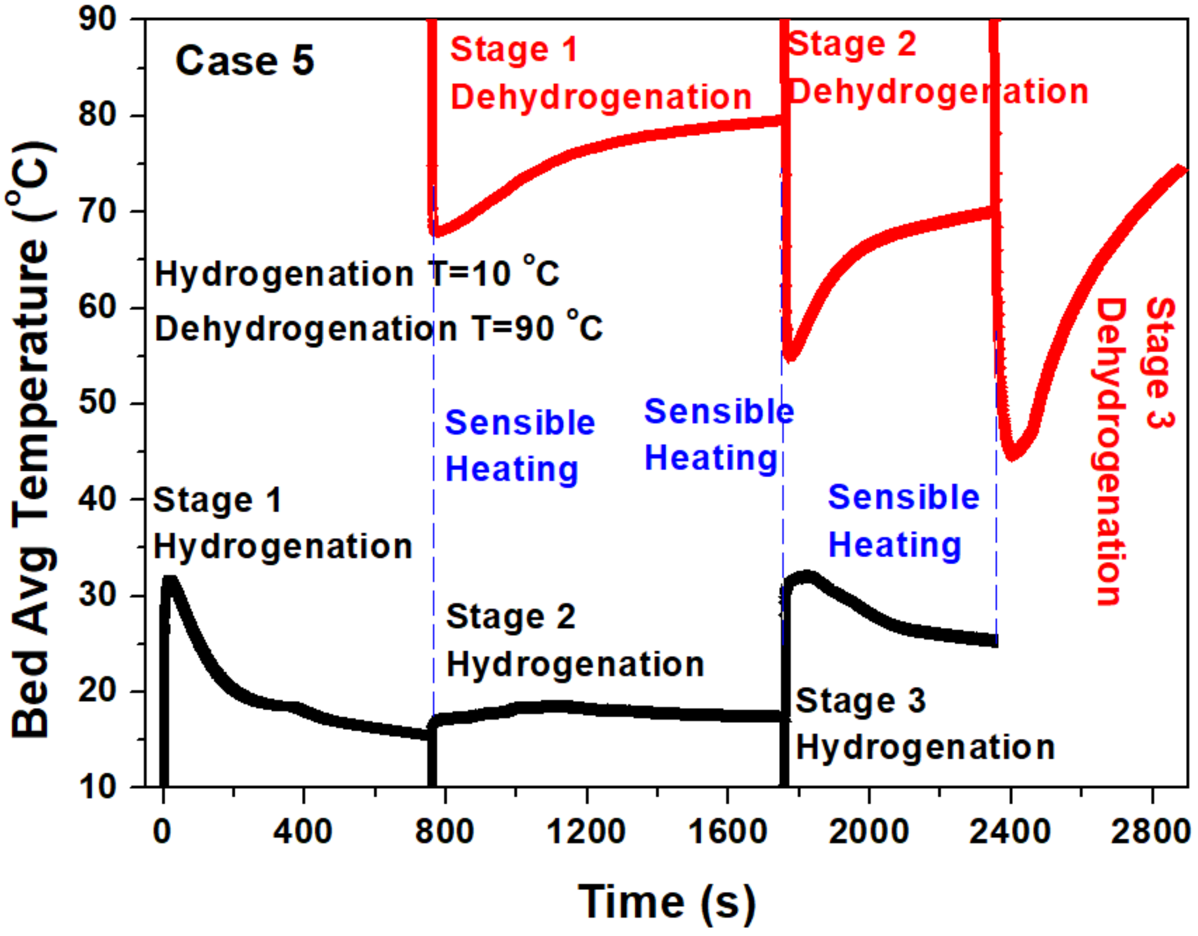

Fig. 6. Bed average temperature profile for the three-stage compression system used in the current study (case No. 5).

The dehydrogenation process thermodynamically is an endothermic reaction, where hydrogen stored in the solid state requires specific amounts of thermal energy to brake the bonds with the material. Thus, for the initial state of the dehydrogenation process, the temperature tends to decrease within the system. After the temperature reaches a minimum value, because of the thermal management, the temperature gradually increases back again.

Fig. 7 presents the pressure evolution for the complete three-stage compression (Case 5). The supply hydrogen pressure is 20 bar at the entrance of stage 1, where a supplier (*e.g electrolyser*) is attached to stage 1 input. As the feedstock is attached to the input, and the supply pressure is constant at 20 bar, it is expected that the pressure during that step will remain at similar levels. The heating of the system after the hydrogenation increases the hydrogen pressure as a contribution of both the desorbed hydrogen and the existing hydrogen in gaseous form. Then the valve between the two systems opens and hydrogen from stage 1 is transferred and stored in stage 2; the driving force for this is the pressure difference between the two stages. During the initial phase of this coupling process, the equilibrium pressure of the releasing tank decreases while the equilibrium pressure of the hydrogenated tank increases sharply due to the rapid kinetics between the two systems. After a certain point, equilibrium is achieved between the two tanks. This process can be seen in detail in the inset of Fig. 7. The pressure at the end of the first coupling reaches a value of almost 70 bar. Then, a second coupling between the reactors of stage 2 and stage 3 takes place. At the end of the second coupling, the pressure reaches the value of almost 220 bar. Finally, the stage 3 reactor releases high-pressure hydrogen to the high-pressure cylinder. For Case 5, the final pressure achieved is 269.28 bar, thus the compression system achieves a compression ratio of 13.46÷1.

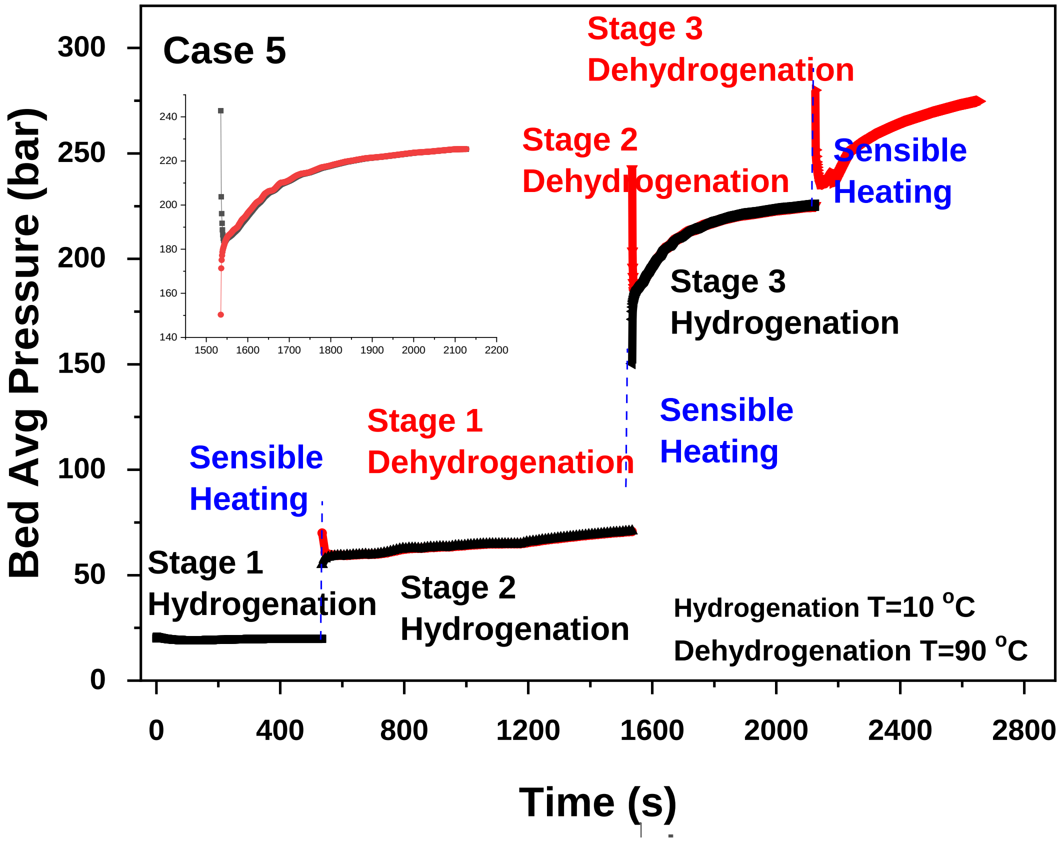

Fig. 7. Bed average pressure profile for the three-stage compression system used in the current study (case No. 5). In the inlaid of Fig. 7, the pressure evolution during the coupling can be seen in detail.

The results from the compression process for all the studied cases in terms of compression ratio (final achieved pressure ÷ initial supply pressure) and duration of compression cycle is presented in Table 4.

Table 4. Results of the compression for all the studied cases in terms of compression ratio and completion time

Case	**P_{supply} (bar)**	**P_{Final} (bar)**	**Compression Ratio**	**Completion Time (s)**
Case 1	20	66.35	3.32÷1	1711
Case 2	20	125.02	6.26÷1	1966
Case 3	20	223.64	11.18÷1	2013
Case 4	50	269.28	5.39÷1	1785
Case 5	20	269.28	13.46÷1	2656

As seen in Table 4, the maximum compression ratio is achieved when the three-stage system is utilised (13.46÷1). However, the duration of the compression time is longer, as it involves an extra stage. Case 3 presents a relatively high compression ratio (11.18÷1) and at the same time the duration time is lower than Case 5 by almost 10 min. In addition, the total compression system is smaller, simpler, lighter and cheaper, as it involves only two reactors instead of three.

The pressure profile for all the studied cases is presented in Fig. 8. For the Cases 1, 2, 3 and 5, the initial pressure is 20 bar, whereas for Case 4, due to the thermodynamic demands of stage 1, the supply pressure is 50 bar.

For Case 4, the initial hydrogenation process lasts more as compared with the rest cases. This behaviour is related to the thermodynamic properties of the stage 1 material for that specific case. The first coupling for all the studied cases last between 540 (Case 4) - 950s (Case 5) and at the end of the coupling the pressure in the system is around 30 bar (Case 1), 58 bar (Case 2), 59 bar (Case 3), 215bar (Case 4) and 59 bar (Case 5). At the end of the final dehydrogenation (except Case 5) the pressure is 66.35 bar (Case 1), 125.02 bar (Case 2), 223.64 bar (Case 3) and 269.28 bar (Case 4).

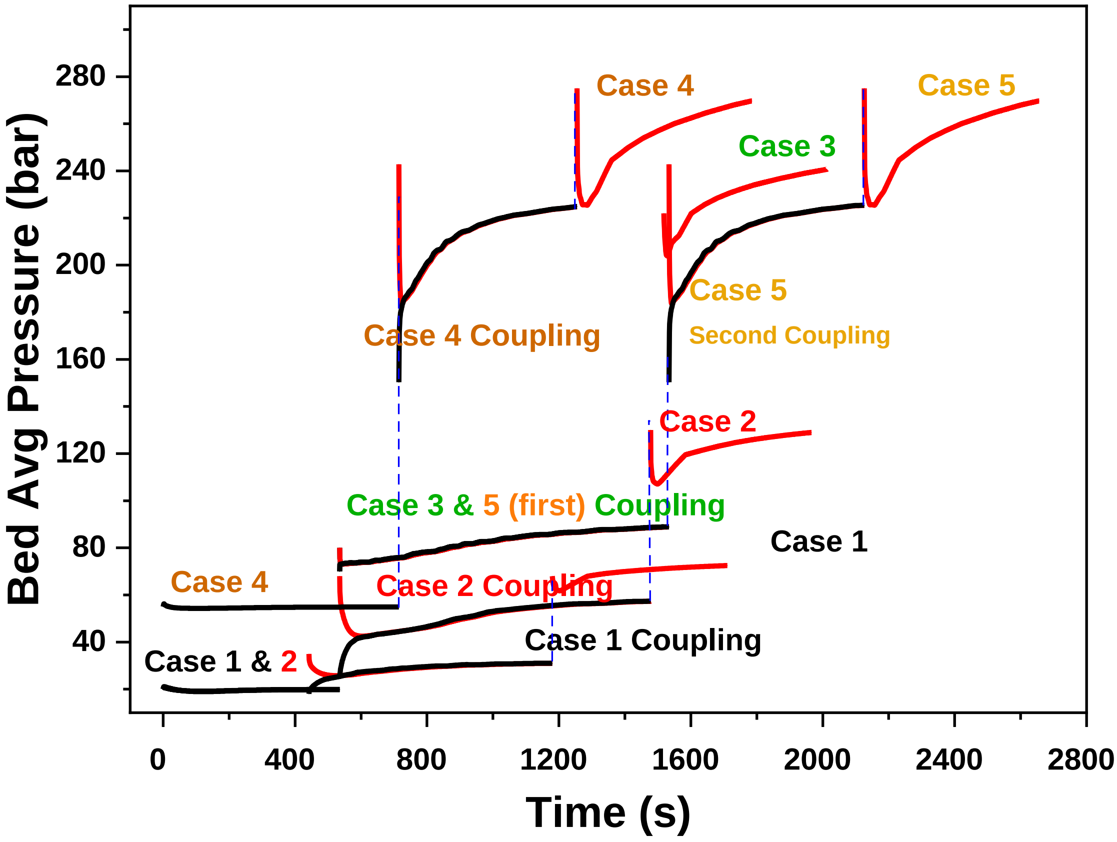

Fig. 8. Comparison of the bed average pressure profiles for all the studied cases

A really important aspect in the design and development of metal hydride tanks, whether the final application is for solid state hydrogen storage or for metal hydride-based hydrogen compression is the thermal management of the tank [26, 69]. In the current study, a helical coil was considered and placed co-centrally inside the tank along with an external shell where the coolant flows as presented in Fig. 3. The length of the metal hydride tanks used in this study was 9.2 m, and it is very important to extract a clear picture regarding the temperature of the metal hydride during the hydrogenation and dehydrogenation at various places of the metal hydride along the length of the tank. It is important to develop a thermal management system to ensure that the cooling/heating is done in a way such that the temperature distribution at each position along the tank will be homogeneous across the tank section (ideally it should be homogeneous everywhere). Fig. 9a, shows five different points along the tank that have been selected for closer inspection (*Point 1: x=0.675 m, Point 2: x=2.675 m, Point 3: x=4.675 m, Point 4: x=6.675 m, Point 5: x=8.675 m, where x=0 m is the inlet point*). The temperature profiles of the five points during the hydrogenation process are presented in Fig. 9b. For Point 1 and Point 2, which are closest to the inlet ($x=0\ m$) the temperature drops in a similar way after the initial ramp due to the exothermic nature of the hydrogen absorption, while for the remaining points the temperature drop takes place at a slower rate. This performance affects the hydrogenation rate across the reactor. Fig. 9c presents the hydrogenation performance of the five points. As the hydrogenation kinetics are heavily affected by the temperature profile within the metal hydride tank, the two closest points to the inlet are reaching 90% of the theoretical maximum hydrogenation capacity almost simultaneously (at 494s and 500s respectively), while Point 3 reaches the 90% level at 585s and Point 4 after 615s. Finally, Point 5, which is close to the end of the cylinder, reaches the 90% level at 782s. The difference in the time required to reach the 90% level between Point 1 and Point 5 is 288s (almost 5 minutes). Based on these outcomes, the thermal management scheme selected and studied in the present case can ensure a relatively homogeneous temperature distribution until the middle of the reactor (Point 3), but after that point the temperature profile begins to change, presenting a slower rate, and as a result, affecting the hydrogenation/dehydrogenation rates. It should be emphasized that the present extended model has the capability (as it also accounts for the cooling / heating fluid flow), as part of future work, to pay particular attention towards the development of a more efficient way to ensure the balance of the temperature evolution inside the reactor. A possible approach might involve the installation of more than one inlets at various points of the tank. For the case described in this study, the temperature was found to be relatively homogeneous for the first two points (Point 1 and Point 2) while Point 3 presented a somewhat slower behavior; thus, another inlet could be designed and installed to cover the second half of the tank to ensure similar temperature behaviour for the whole reactor. By achieving that, the results presented in Figs. 5-8 are expected to become more favourable, as the bed average temperature and pressure have been considered in the figures. Furthermore, other design modifications regarding heat transfer issues (e.g. fluid flowrates, heat exchanger features and geometry, etc.) can be examined with the use of the present extended model to improve the thermal characteristics of the metal hydride bed and, ultimately, to achieve higher MHHC capacities in terms of hydrogen flowrate.

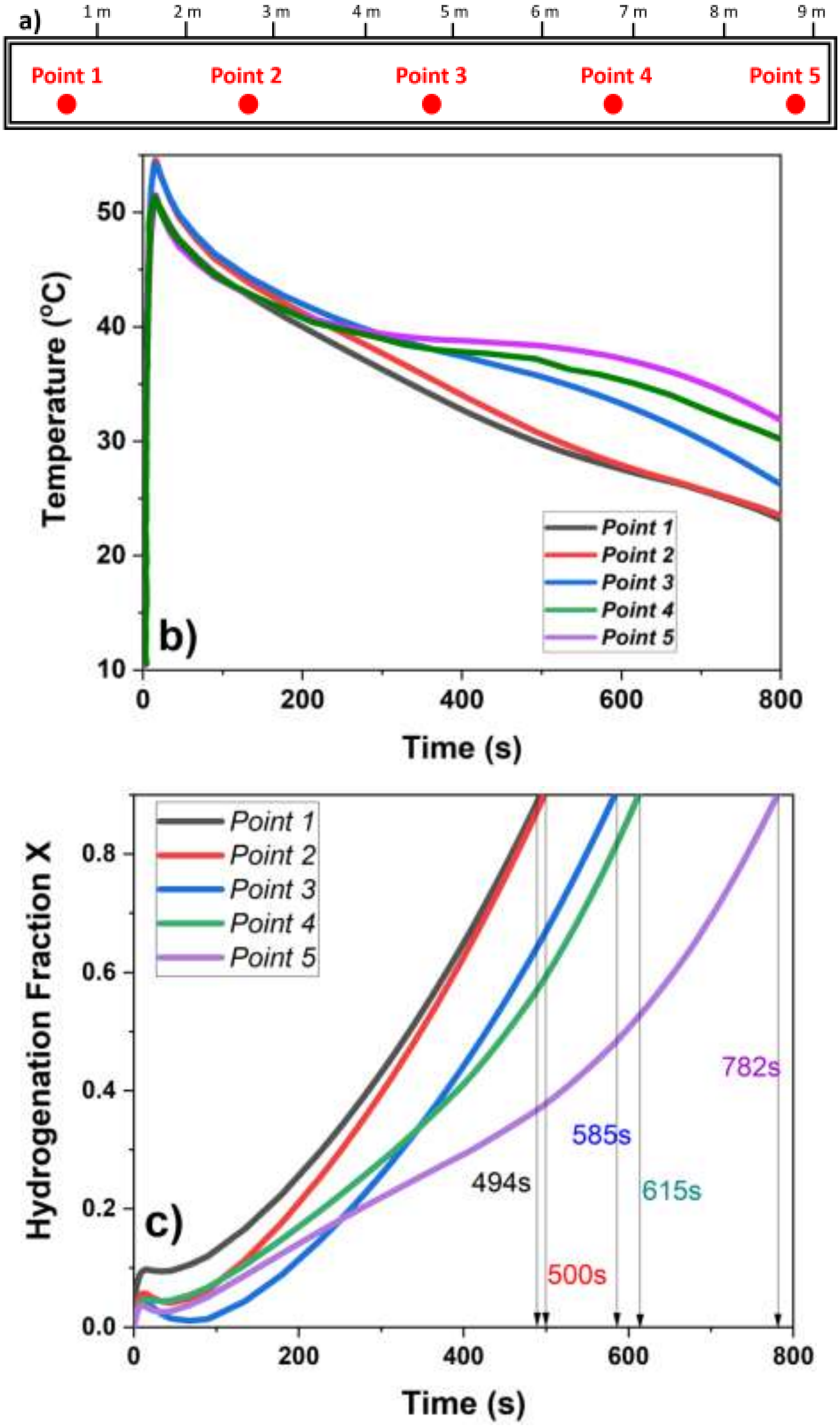

Fig. 9. Position of the five points selected for the study of the temperature distribution across the hydride tank (9a). Temperature profile (9b) and hydrogenation behaviour (9c) of the five selected points

4.2 Thermal Energy Demand

A compression system that is based on the utilisation of metal hydrides is a thermally-driven process. Certain amounts of thermal energy are necessary for the operation of the compressor. The thermal energy is required for the heating and the cooling of the metal hydrides, the metal hydride tanks and at the same time to initiate and maintain the hydrogen storage and release. For each dehydrogenation process, there are two types of thermal energy required. The first type is related to the energy to heat both the SS walls of the tank as well as the material and the SS helical shell. The second type of thermal energy is the energy required to release the stored hydrogen from the hydride. The same types of thermal energy are also required for the hydrogenation process, only now the requirement is to cool the walls, helical shell and the material and to store hydrogen to form the hydride phase. The total amount of thermal energy required for the compression process is updated by:

$$Q_t = Q_{sens} + Q_{lat} \tag{24}$$

In Eq. 24, the term Q_{sens} *(J)* refers to the thermal energy that is exchanged between the system and its environment to cause a temperature difference ΔT *(K)* to the system. The sensible thermal requirements can be calculated by taking into account the mass of the material to be heated/cooled *(kg)*, the heat capacity of the material *(J/Kg/K)* and the temperature difference *(K)* that this amount of heat causes; the Q_{sens} is updated by the following:

$$Q_{sens} = \sum_{i=1}^{N} (m_i \cdot C_i) \cdot \Delta \mathrm{T} \tag{25}$$

In addition, the term Q_{lat} *(J)* is the amount of heat that is necessary to remove/store hydrogen from/to the material and is directly related to the thermodynamic properties of the material and the amount of hydrogen to be stored/released. The latent heat requirements are provided by the following expression:

$$Q_{lat} = \Delta \mathrm{H} \cdot n_{H_2} \tag{26}$$

In Eq. 26, ΔH *(J/mol)* is the enthalpy change for the hydride formation/deformation and n_{H2} is the amount of hydrogen *(mol stored/released to/from the hydride).*

Table 5 presents the thermal energy requirements for the sensible heating/cooling, the latent heating/cooling requirements and also a small amount of energy that is necessary to be provided to the desorbed hydrogen. For the calculations, the mass of the SS walls of the tanks and the mass of the spiral heat exchanger have been calculated as 181.42 and 150.03 kg respectively introduced.

Table 5. Total thermal energy requirements for all the compression cases

Case	Total Q_{sens} (MJ)	Total Q_{lat} (MJ)	Thermal Energy for Hydrogen (MJ)	Total thermal energy (MJ)	Compression Ratio	Compression Duration (s)
Case 1	56.23	25.06	3.06	84.35	3.32÷1	1711
Case 2	54.46	23.26	3.44	81.16	6.26÷1	1966
Case 3	54.32	21.72	3.82	79.86	11.18÷1	2013
Case 4	54.01	19.35	4.02	77.38	5.39÷1	1785
Case 5	81.31	31.16	4.89	117.36	13.46÷1	2656

The total sensible thermal requirements are of similar levels for the Cases 1-4, where the temperature difference is the same (80 ^{o}C), the mass of the SS tank is also the same. The main differences are the mass and the thermodynamic properties of the materials of each stage. As expected, the sensible thermal requirements for Case 5 are higher, as there is the involvement of an extra compression stage. Case 4 requires the least amount of thermal energy for its operation, but it presents two main drawbacks; relatively low compression ratio and the relatively high supply pressure requirement. On the other hand, Case 5 presents the highest compression ratio along with the maximum energy demand and duration. Case 3 presents a relatively high compression ratio with lower thermal energy requirements than Case 5 and faster operation.

For comparison purposes of all the considered cases, a *comparison ratio* is introduced: the ratio between the thermal energy demand and the compression ratio. Fig. 10 presents this comparison ratio against the total duration of each compression case. Between all the studied cases, Case 1 presents the highest value of the comparison ratio (25.41), whereas Case 2 and Case 4 present relatively lower values (12.96 and 14.36 respectively). The lowest values and as a consequence the more effective compression systems are the compressors of Case 3 and Case 5 (7.14 and 8.72 respectively).

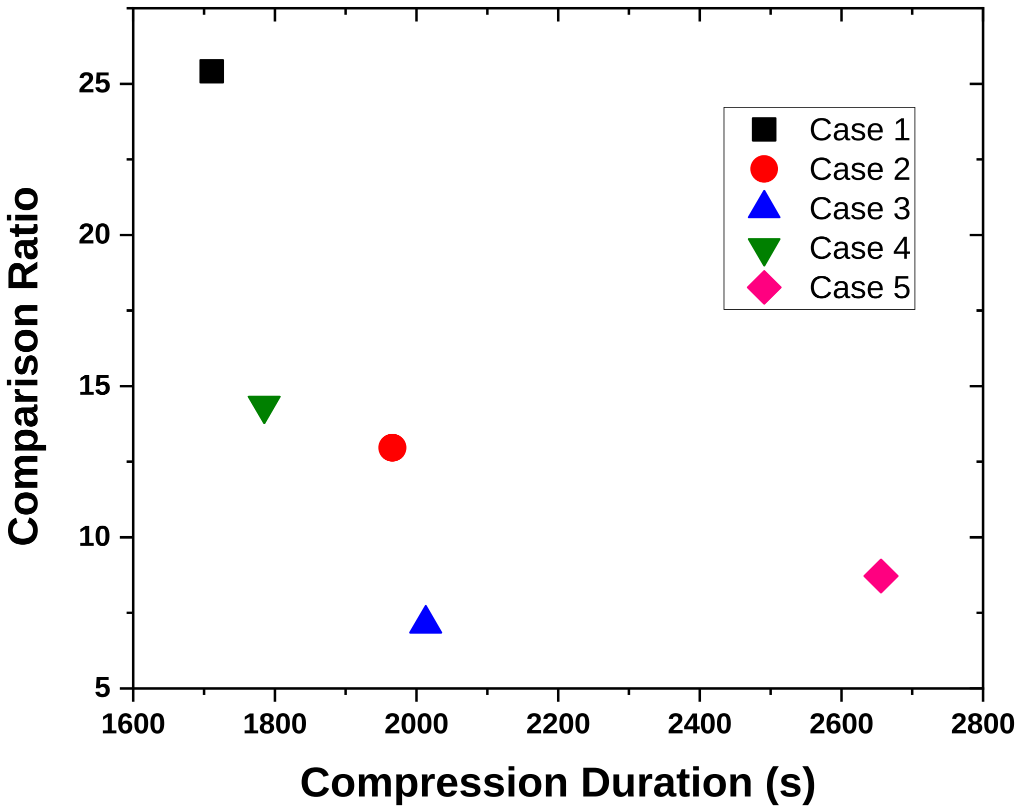

Fig. 10. Comparison of the effectiveness of all the studied cases

4.3 Compressor Efficiency

The metal hydride-based compressors in principle are heat engines, as they convert heat to work. For the case where the thermal energy reservoirs (heat sink and heat source) are based on renewable sources, such as solar panels and photovoltaic systems, the efficiency is not of major importance. In the present work, that is the reason for the selection of that specific operation temperature range (10 - 90 ^{o}C).

However, for the development of the total picture regarding the utilisation of metal hydride hydrogen compression systems and the evaluation of their performance, an analysis on the efficiency is considered. For the five cases described in the study, the compression ratios achieved at each compression system were *3.32 – 6.26 – 11.18 – 5.39 and 13.46* respectively. The required work to achieve this compression ratio was calculated by introducing four main scenarios. The first scenario is the *isothermal compression*, the second is the *isentropic* *compression*, the third is the *polytropic compression* and the final scenario deals with a 75% *isentropic compression*, which is an approximation that represents real-life applications.

For the first scenario (isothermal process) the work during the compression is given by the following expression:

$$W_{iso} = P_{in} \cdot V_l \cdot ln r_p \tag{27}$$

In Eq. 27, V_l (m^3/kg) is the hydrogen's specific volume, P_{in} (bar) is the initial supply pressure and r_p is the compression ratio achieved.

The isentropic work for the second scenario is given by the following equation:

$$W_s = \frac{k}{k-1} \cdot P_{in} \cdot V_l \cdot \left(r_p^{\frac{k-1}{k}} - 1 \right) \tag{28}$$

In Eq. 28, k is the adiabatic ratio (C_p/C_v), P_{in} (bar) is the initial supply pressure, V_l (m^3/kg) is the hydrogen's specific volume and r_p is the compression ratio achieved.

The work during the polytropic process is given by:

$$W_{pol} = \frac{n_p}{n_p-1} \cdot P_{in} \cdot V_l \cdot \left(r_p^{\frac{k-1}{k}} - 1 \right) \tag{29}$$

In Eq. 29, n_p is the polytropic coefficient. In addition, the definition of the thermal efficiency for any heat engine is given by:

$$\eta_{th} = \frac{W}{Q} \cdot 100 \tag{30}$$

In the present analysis, Q (J) represents the thermal energy requirements of the compressor, as described in *4.2*. Finally, the second law efficiency is the ratio between the actual efficiency and the Carnot efficiency:

$$\eta_c = \frac{n_{th}}{n_{carnot}} \tag{31}$$

The Carnot efficiency is given by the following expression:

$$\eta = 1 - \frac{T_{low}}{T_{high}} \tag{32}$$

Table 6 presents the efficiency calculations for all the compression scenarios.

Table 6. Theoretical calculations for the compressor efficiencies

Case	Isothermal Efficiency	Isothermal η_c	Isentropic Efficiency	Isentropic η_c	Polytropic Efficiency	Polytropic η_c	Adiabatic Irreversible	Isentropic Reversible n_c
1	1.53	6.92	1.85	8.41	1.61	7.33	1.09	4.91
2	2.41	10.92	3.24	14.70	2.83	12.82	1.89	8.58
3	3.11	14.11	4.56	20.71	3.98	18.07	2.67	12.09
4	5.96	27.06	7.89	35.80	6.89	31.23	1.85	8.36
5	2.37	10.72	3.63	16.48	3.17	14.38	2.12	9.62

According to the results extracted from the previous analysis, Case 4 presents the highest efficiency for all the studied scenarios. However, according to the analysis done in Fig. 9, Case 4 presents a low compression ratio and at the same time requires a large initial supply pressure. The main reason for the relatively large efficiency values is that in Eq. 21, Eq. 22 and Eq. 23, the parameter P_{in} is 50 bar for Case 4, while for the rest cases is 20 bar. This indicates that the comparison between Case 4 and the rest compression cases doesn't provide safe conclusions, as the compared systems should operate under the same conditions.

For the remaining cases with the initial supply pressure of 20 bar, Case 3 presents the highest efficiency for all the studied cases, followed by the efficiency values for Case 5, Case 2 and Case 1 respectively. The above results are in good agreement with the analysis done in Fig. 9. The results indicate that although the compression system described by Case 3 doesn't reach the highest pressure and doesn't achieve the highest compression ratio, it presents the highest possible efficiency as compared with the rest compressors operating under the same conditions.

5. Conclusions

A numerical approach to describe the operation of five metal-hydride based compression systems is introduced, validated and described in terms of temperature and pressure profile, compression ratio, thermal energy requirements and compression efficiency. Four cases were based on two-stage operation and for comparison purposes, a three-stage compression system was introduced. The operational temperature was 10 °C for the hydrogenation and 90 °C for the dehydrogenation. The initial supply hydrogen pressure was 20 bar, whereas for the compression system of Case 4, the initial supply pressure was 50 bar due to the thermodynamic requirements. The main conclusions reached in the current study are the following:

- The maximum pressure values achieved when the temperature conditions are 10 °C (hydrogenation) – 90 °C (dehydrogenation) range between 270 bar for the three-stage compression system and 67 bar for Case 1.
- To increase the final delivery pressure, the dehydrogenation temperature must be increased, but this will introduce two main challenges: The usage of different medium instead of water to heat / cool the reactors which will make the system more complicated and expensive. The second challenge is that at high temperatures it may not be easy to utilise solely renewables, a fact that will affect significantly the efficiency and the cost of the compressor.
- Almost all the compression cases introduced in the current study, present similar levels of thermal energy requirements which range between 312-340.12 kJ/molH_2 for the two-stage systems while for the three-stage system reach 473 kJ/molH_2. The duration of the compression cycle was also at relatively similar levels for the different Cases.
- The compression under 10 °C (hydrogenation) – 90 °C (dehydrogenation) for the most prominent two-stage compression case (Case 3) showed a compression ratio of 11.18:1, an isentropic efficiency of 4.54% and second law efficiency of 20.71%, with a thermal energy demand of 322 kJ/molH_2 and a cycle time of 2013 s, while for the three-stage compression system the compression ratio was 13.46:1 with a lower isentropic efficiency of 3.63% and second law efficiency of 16.48%, and higher values of thermal energy requirement (473 kJ/molH_2) and higher compression duration (2656 s).
- Future studies regarding the thermal management should consider the fact that when designing large-scale reactors the temperature distribution should be kept as homogeneous as possible throughout the tank, in order to ensure the maximum performance during operation. The present model allows for such studies and therefore possesses enhanced capabilities for practical MHHC design considerations.

Acknowledgments: ES, CC, GK and AS acknowledge co-financing by the European Regional Development Fund of the EU and Greek national funds under the call RESEARCH – CREATE – INNOVATE (project H2CYRUS / T2EDK-02151).

Nomenclature		k	*adiabatic ratio* (C_p/C_v)
C	*AbsorptionDesorption Reaction Constant,* s^{-1}	n_p	*Polytropic Coefficient*
C_p	*Specific Heat, J/kg-K*	n_{th}	*Thermal Efficiency*
E_a	*Activation Energy for Absorption,* $J/molH_2$	n_{carn}	*Carnot Efficiency*
E_d	*Activation Energy for Desorption,* $J/molH_2$	**Subscripts**	
h	*Heat Transfer Coefficient,* W/m^2K	a	*Absorption*
k	*Thermal Conductivity, W/m-K*	A	*Reactor A*
K	*Permeability,* m^2	B	*Reactor B*
M	*Molecular Weight, kg/mol*	d	*Desorption*
$\dot{m}$	*Absorption/Desorption Kinetics,* kg/m^3*-s*	e	*Effective*
n	*moles*	eq	*Equilibrium*
P	*Pressure, Pa*	g	*Gas*
R	*Gas Universal Constant, J/mol-K*	i	*Initial*
t	*Time, s*	s	*Solid*
T	*Temperature, K*	ss	*Saturation*
v	*Velocity, m/s*	f	*Fluid*
V	*Volume,* m^3	**Greek Letters**	
C	*Fitting Coefficient*	ε	*Porosity*
Z	*Compressibility Factor*	μ	*Dynamic Viscosity, kg/ms*
Y	*Hysteresis*	ρ	*Density,* kg/m^3
Q	*Thermal Energy, J*	ΔH	*Reaction Enthalpy, J/mol*
W	*Work, J*	ΔS	*Reaction Entropy, J/mol-K*
V_l	*Specific Volume,* m^3/kg	η **(eta)**	*Thermal Efficiency*
r_p	*Compression Ratio*	**Symbols**	
$\vec{V}$	*Velocity Vector (m/s)*	$\sum$	*Summary*
Pr	*Prandtl Number*	∇	*Nabla*
L	*Length (m)*		

References

[1] Energy Information Administration, International Energy Outlook, 2017

[2] Makridis SS, Gkanas EI, Panagakos G, Kikkinides ES, Stubos AK, Wagener P, et al. Polymer-stable magnesium nanocomposites prepared by laser ablation for efficient hydrogen storage. Int J Hydrogen Energy 2013;38; 11530-11535. https://doi.org/ 10.1016/j.ijhydene.2013.04.031.

[3] Inventory of U.S. Greenhouse Gas Emissions and Sinks: 1990–2017.

[4] Ozturk M, Dincer I. An integrated system for ammonia production from renewable hydrogen: A case study. Int J Hydrogen Energy 2021;46:5918–25. https://doi.org/https://doi.org/10.1016/j.ijhydene.2019.12.127.

[5] European Environment Agency (EEA) https://www.eea.europa.eu/ (last accessed 22/04/2020)

[6] A. Chapman, K. Itaoka, H. Farabi-Asl, Y. Fujii, and M. Nakahara, "Societal penetration of hydrogen into the future energy system: Impacts of policy, technology and carbon targets," Int. J. Hydrogen Energy, vol. 45, no. 7, pp. 3883–3898, 2020.

[7] Qureshy AMMI, Dincer I. A new integrated renewable energy system for clean electricity and hydrogen fuel production. Int J Hydrogen Energy 2020;45:20944–55. https://doi.org/https://doi.org/10.1016/j.ijhydene.2020.04.218.

[8] Gkanas EI. Metal hydrides: Modeling of metal hydrides to be operated in a fuel cell. Portable Hydrog. Energy Syst., 2018. doi:10.1016/b978-0-12-813128-2.00005-

[9] Yartys VA, Lototskyy M V., Akiba E, Albert R, Antonov VE, Ares JR, et al. Magnesium based materials for hydrogen based energy storage: Past, present and future. Int J Hydrogen Energy 2019. doi:10.1016/j.ijhydene.2018.12.212.

[10] Khzouz M, Gkanas EI, Shao J, Sher F, Beherskyi D, El-Kharouf A, et al. Life Cycle Costing Analysis: Tools and Applications for Determining Hydrogen Production Cost for Fuel Cell Vehicle Technology. Energies 2020. https://doi.org/10.3390/en13153783.

[11] Khzouz M, Gkanas EI, Girella A, Statheros T, Milanese C. Sustainable hydrogen production via LiH hydrolysis for unmanned air vehicle (UAV) applications. Int J Hydrogen Energy 2020;45:5384–94. https://doi.org/https://doi.org/10.1016/j.ijhydene.2019.05.189

[12] Iordache M, Schitea D, Iordache I. Hydrogen refuelling station infrastructure roll-up, an indicative assessment of the commercial viability and profitability in the Member States of Europe Union. Int J Hydrogen Energy 2017. doi:10.1016/j.ijhydene.2017.09.146.

[13] Yilmaz F, Ozturk M, Selbas R. Design and thermodynamic modeling of a renewable energy based plant for hydrogen production and compression. Int J Hydrogen Energy 2020;45:26126–37. https://doi.org/https://doi.org/10.1016/j.ijhydene.2019.12.133.

[14] Apostolou D, Enevoldsen P, Xydis G. Supporting green Urban mobility – The case of a small-scale autonomous hydrogen refuelling station. Int J Hydrogen Energy 2019. doi:10.1016/j.ijhydene.2018.11.197

[15] Riedl SM. Development of a Hydrogen Refueling Station Design Tool. Int J Hydrogen Energy 2020;45:1–9. doi:https://doi.org/10.1016/j.ijhydene.2019.09.234.

[16] Gkanas EI, Khzouz M. Metal Hydride Hydrogen Compression Systems - Materials, Applications and Numerical Analysis. Hydrog. Storage Technol., 2018. doi:10.1002/9781119460572.ch1.

[17] Stamatakis E, Zoulias E, Tzamalis G, Massina Z, Analytis V, Christodoulou C, et al. Metal hydride hydrogen compressors: Current developments and early markets. Renew Energy 2018. doi:10.1016/j.renene.2018.04.073.

[18] Lototskyy M, Klochko Y, Davids MW, Pickering L, Swanepoel D, Louw G, et al. Industrial-scale metal hydride hydrogen compressors developed at the South African Institute for Advanced Materials Chemistry. Mater. Today Proc., 2018. doi:10.1016/j.matpr.2017.12.383.

[19] Gkanas EI, Grant DM, Khzouz M, Stuart AD, Manickam K, Walker GS. Efficient hydrogen storage in up-scale metal hydride tanks as possible metal hydride compression agents equipped with aluminium extended surfaces. Int J Hydrogen Energy 2016;41. doi:10.1016/j.ijhydene.2016.04.035.

[20] Ozsaban M, Midilli A. A parametric study on exergetic sustainability aspects of high-pressure hydrogen gas compression. Int J Hydrogen Energy 2016;41:5321–34. https://doi.org/https://doi.org/10.1016/j.ijhydene.2016.01.130.

[21] Witkowski A, Rusin A, Majkut M, Stolecka K. Comprehensive analysis of hydrogen compression and pipeline transportation from thermodynamics and safety aspects. Energy 2017. doi:10.1016/j.energy.2017.05.141.

[22] uthukumar P, Prakash Maiya M, Srinivasa Murthy S. Performance tests on a thermally operated hydrogen compressor. Int J Hydrogen Energy 2008. doi:10.1016/j.ijhydene.2007.07.019.

[23] Rusanov A V, Solovey V V, Lototskyy M V. Thermodynamic features of metal hydride thermal sorption compressors and perspectives of their application in hydrogen liquefaction systems. J Phys Energy 2020. https://doi.org/10.1088/2515-7655/ab7bf4.

[24] Bellosta von Colbe J, Ares J-R, Barale J, Baricco M, Buckley C, Capurso G, et al. Application of hydrides in hydrogen storage and compression: Achievements, outlook and perspectives. Int J Hydrogen Energy 2019;44:7780–808. https://doi.org/https://doi.org/10.1016/j.ijhydene.2019.01.104.

[25] Dehouche Z, Grimard N, Laurencelle F, Goyette J, Bose TK. Hydride alloys properties investigations for hydrogen sorption compressor. J Alloys Compd 2005. doi:10.1016/j.jallcom.2005.01.029.
[26] Lototskyy M, Satya Sekhar B, Muthukumar P, Linkov V, Pollet BG. Niche applications of metal hydrides and related thermal management issues. J Alloys Compd 2015. doi:10.1016/j.jallcom.2014.12.271.
[27] Kelly NA, Girdwood R. Evaluation of a thermally-driven metal-hydride-based hydrogen compressor. Int J Hydrogen Energy 2012. doi:10.1016/j.ijhydene.2012.04.088.
[28] Lototskyy M, Tolj I, Klochko Y, Davids MW, Swanepoel D, Linkov V. Metal hydride hydrogen storage tank for fuel cell utility vehicles. Int J Hydrogen Energy 2020. doi:10.1016/j.ijhydene.2019.04.124.
[29] Lototskyy M V., Yartys VA, Pollet BG, Bowman RC. Metal hydride hydrogen compressors: A review. Int. J. Hydrogen Energy, 2014. doi:10.1016/j.ijhydene.2014.01.158.
[30] Karagiorgis G, Christodoulou CN, von Storch H, Tzamalis G, Deligiannis K, Hadjipetrou D, et al. Design, development, construction and operation of a novel metal hydride compressor. Int J Hydrogen Energy 2017. doi:10.1016/j.ijhydene.2017.03.195.
[31] Yartys VA, Lototskyy M, Linkov V, Grant D, Stuart A, Eriksen J, et al. Metal hydride hydrogen compression: recent advances and future prospects. Appl Phys A Mater Sci Process 2016. doi:10.1007/s00339-016-9863-7.
[32] Laurencelle F, Dehouche Z, Morin F, Goyette J. Experimental study on a metal hydride-based hydrogen compressor. J Alloys Compd 2009. doi:10.1016/j.jallcom.2008.08.007.
[33] Gkanas EI, Makridis SS, Stubos AK. Modeling and simulation for absorption-desorption cyclic process on a three-stage metal hydride hydrogen compressor. Comput. Aided Chem. Eng., 2013. doi:10.1016/B978-0-444-63234-0.50064-6.
[34] Lototskyy M V, Tolj I, Davids MW, Klochko Y V, Parsons A, Swanepoel D, et al. Metal hydride hydrogen storage and supply systems for electric forklift with low-temperature proton exchange membrane fuel cell power module. Int J Hydrogen Energy 2016;41:13831–42. doi:https://doi.org/10.1016/j.ijhydene.2016.01.148.
[35] Gkanas EI, Grant DM, Stuart AD, Eastwick CN, Book D, Nayebossadri S, et al. Numerical study on a two-stage Metal Hydride Hydrogen Compression system. J Alloys Compd 2015;645. doi:10.1016/j.jallcom.2015.03.123.
[36] Gupta S, Sharma VK. Performance investigation of a multi-stage sorption hydrogen compressor. Int J Hydrogen Energy 2021;46:1056–75. https://doi.org/https://doi.org/10.1016/j.ijhydene.2020.09.249.
[37] Bowman RC, Fultz B. Metallic hydrides I: Hydrogen storage and other gas-phase applications. MRS Bull 2002. doi:10.1557/mrs2002.223.
[38] Sandrock G. Panoramic overview of hydrogen storage alloys from a gas reaction point of view. J Alloys Compd 1999. doi:10.1016/S0925-8388(99)00384-9.
[39] Bowman RC, Witham C, Fultz B, Ratnakumar B V., Ellis TW, Anderson IE. Hydriding behavior of gas-atomized AB5 alloys. J Alloys Compd 1997. doi:10.1016/s0925-8388(96)02929-5.
[40] Bowman RC, Payzant EA, Wilson PR, Pearson DP, Ledovskikh A, Danilov D, et al. Characterization and analyses of degradation and recovery of LaNi 4.78Sn0.22 hydrides following thermal aging. J Alloys Compd 2013. doi:10.1016/j.jallcom.2013.03.129.
[41] Sharma VK, Anil Kumar E. Thermodynamic Analysis of Two Stage Metal Hydride Based Hydrogen Compressor. Mater Today Proc 2018;5:23218–23. doi:https://doi.org/10.1016/j.matpr.2018.11.053.
[42] Uchida H. Surface processes of H2 on rare earth based hydrogen storage alloys with various surface modifications. Int J Hydrogen Energy 1999. doi:10.1016/S0360-3199(98)00160-8.
[43] Pickering L, Reed D, Bevan AI, Book D. Ti-V-Mn based metal hydrides for hydrogen compression applications. J Alloys Compd 2015. doi:10.1016/j.jallcom.2014.12.098.
[44] Bhogilla SS. Design of a AB2-metal hydride cylindrical tank for renewable energy storage. J Energy Storage 2017. doi:10.1016/j.est.2017.10.012.
[45] Koultoukis ED, Makridis SS, Pavlidou E, de Rango P, Stubos AK. Investigation of ZrFe2-type materials for metal hydride hydrogen compressor systems by substituting Fe with Cr or V. Int J Hydrogen Energy 2014;39:21380–5. doi:https://doi.org/10.1016/j.ijhydene.2014.03.184.
[46] Muthukumar P, Maiya MP, Murthy SS. Experiments on a metal hydride based hydrogen compressor. Int J Hydrogen Energy 2005. doi:10.1016/j.ijhydene.2004.09.003.
[47] Pickering L, Lototskyy M V., Davids MW, Sita C, Linkov V. Induction melted AB2-Type metal hydrides for hydrogen storage and compression applications. Mater. Today Proc., 2018. doi:10.1016/j.matpr.2017.12.378
[48] Ivey DG, Northwood DO. Storing hydrogen in AB2 laves-type compounds. Zeitschrift Fur Phys Chemie 1986. doi:10.1524/zpch.1986.147.1_2.191.
[49] Gkanas EI, Khzouz M. Numerical analysis of candidate materials for multi-stage metal hydride hydrogen compression processes. Renew Energy 2017. doi:10.1016/j.renene.2017.04.037.
[50] Hardy BJ, Anton DL. Hierarchical methodology for modeling hydrogen storage systems. Part I: Scoping models. Int J Hydrogen Energy 2009. doi:10.1016/j.ijhydene.2008.12.070.
[51] Askri F, Jemni A, Ben Nasrallah S. Study of two-dimensional and dynamic heat and mass transfer in a metal-hydrogen reactor. Int J Hydrogen Energy 2003. doi:10.1016/S0360-3199(02)00141-6.

[52] Kikkinides ES, Georgiadis MC, Stubos AK. Dynamic modelling and optimization of hydrogen storage in metal hydride beds. Energy 2006. doi:10.1016/j.energy.2005.10.036.
[53] Muthukumar P, Madhavakrishna U, Dewan A. Parametric studies on a metal hydride based hydrogen storage device. Int J Hydrogen Energy 2007. doi:10.1016/j.ijhydene.2007.08.010.
[54] Gkanas EI, Khzouz M, Panagakos G, Statheros T, Mihalakakou G, Siasos GI, et al. Hydrogenation behavior in rectangular metal hydride tanks under effective heat management processes for green building applications. Energy 2018. doi:10.1016/j.energy.2017.10.040.
[55] Lototskyy M V, Yartys VA, Tarasov BP, Denys R V, Eriksen J, Bocharnikov MS, et al. Modelling of metal hydride hydrogen compressors from thermodynamics of hydrogen – Metal interactions viewpoint: Part II. Assessment of the performance of metal hydride compressors. Int J Hydrogen Energy 2021;46:2339–50. https://doi.org/https://doi.org/10.1016/j.ijhydene.2020.10.080.
[56] Fragiacomo P, Genovese M. Developing a mathematical tool for hydrogen production, compression and storage. Int J Hydrogen Energy 2020;45:17685–701. https://doi.org/https://doi.org/10.1016/j.ijhydene.2020.04.269.
[57] Lototskyy M V, Yartys VA, Tarasov BP, Davids MW, Denys RV, Sun Tai. Modelling of metal hydride hydrogen compressors from thermodynamics of hydrogen – Metal interactions viewpoint: Part I. Assessment of the performance of metal hydride materials. Int J Hydrogen Energy 2021;46:2330–38. https://doi.org/10.1016/j.ijhydene.2020.10.090.
[58] Gkanas EI, Statheros T, Khzouz M. Heat management on rectangular metal hydride tanks for green building applications. Int J Hydrogen Energy 2019;44:19267–74. https://doi.org/https://doi.org/10.1016/j.ijhydene.2018.06.030.
[59] K.B. Minko, M.S. Bocharnikov, Y.B. Yanenko, M. V. Lototskyy, A. Kolesnikov, B.P. Tarasov, Numerical and experimental study of heat-and-mass transfer processes in two-stage metal hydride hydrogen compressor, Int. J. Hydrogen Energy. (2018). doi:10.1016/j.ijhydene.2018.09.211.
[60] Muthukumar P, Singh Patel K, Sachan P, Singhal N. Computational study on metal hydride based three-stage hydrogen compressor. Int. J. Hydrogen Energy, 2012. doi:10.1016/j.ijhydene.2011.05.104.
[61] Galvis E AR, Leardini F, Bodega J, Ares JR, Fernandez JF. Realistic simulation in a single stage hydrogen compressor based on AB2 alloys. Int J Hydrogen Energy 2016. doi:10.1016/j.ijhydene.2016.01.125.
[62] Gkanas EI, Christodoulou CN, Tzamalis G, Stamatakis E, Chroneos A, Deligiannis K, et al. Numerical investigation on the operation and energy demand of a seven-stage metal hydride hydrogen compression system for Hydrogen Refuelling Stations. Renewable Energy 2020. doi:10.1016/j.renene.2019.08.104.
[63] Pons M, Dantzer P. Heat Transfer in Hydride Packed Beds. II. A New Experimental Technique and Results on LaNi5 Powder. Zeitschrift Fur Phys Chemie 1994. doi:10.1524/zpch.1994.183.Part_1_2.213.
[64] Mohammadshahi SS, Gould T, Gray EMA, Webb CJ. An improved model for metal-hydrogen storage tanks - Part 1: Model development. Int J Hydrogen Energy 2016. doi:10.1016/j.ijhydene.2015.12.050.
[65] Lin X, Yang H, Zhu Q, Li Q. Numerical simulation of a metal hydride tank with LaNi4.25Al0.75 using a novel kinetic model at constant flows. Chem Eng J 2020;401:126115. https://doi.org/https://doi.org/10.1016/j.cej.2020.126115.
[66] Nishizaki T, Miyamoto K, Yoshida K. Coefficients of performance of hydride heat pumps. J Less-Common Met 1983. doi:10.1016/0022-5088(83)90372-7.
[67] Gkanas EI, Makridis SS. Effective thermal management of a cylindrical MgH2 tank including thermal coupling with an operating SOFC and the usage of extended surfaces during the dehydrogenation process. Int J Hydrogen Energy 2016;41:5693–708. https://doi.org/https://doi.org/10.1016/j.ijhydene.2016.01.165.
[68] Dornheim M, Thermodynamics of Metal Hydrides: Tailoring Reaction Enthalpies of Hydrogen Storage Materials, Thermodynamics - Interaction Studies - Solids, Liquids and Gases, Juan Carlos Moreno-Pirajan, IntechOpen, 2011, DOI: 10.5772/21662.
[69] Tarasov BP, Fursikov P V, Volodin AA, Bocharnikov MS, Shimkus YY, Kashin AM, et al. Metal hydride hydrogen storage and compression systems for energy storage technologies. Int J Hydrogen Energy 2020. https://doi.org/https://doi.org/10.1016/j.ijhydene.2020.07.085.

Supplementary Data

S1. P-c-T isotherms for all the materials used in this study, along with the comparison of all the isotherms at 10ºC and 80ºC.

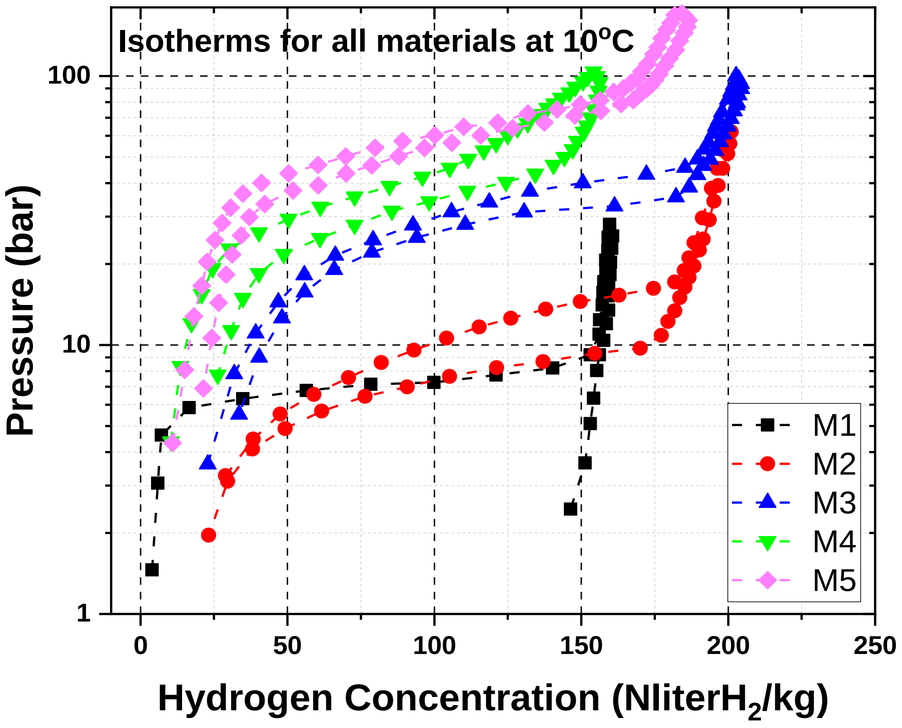

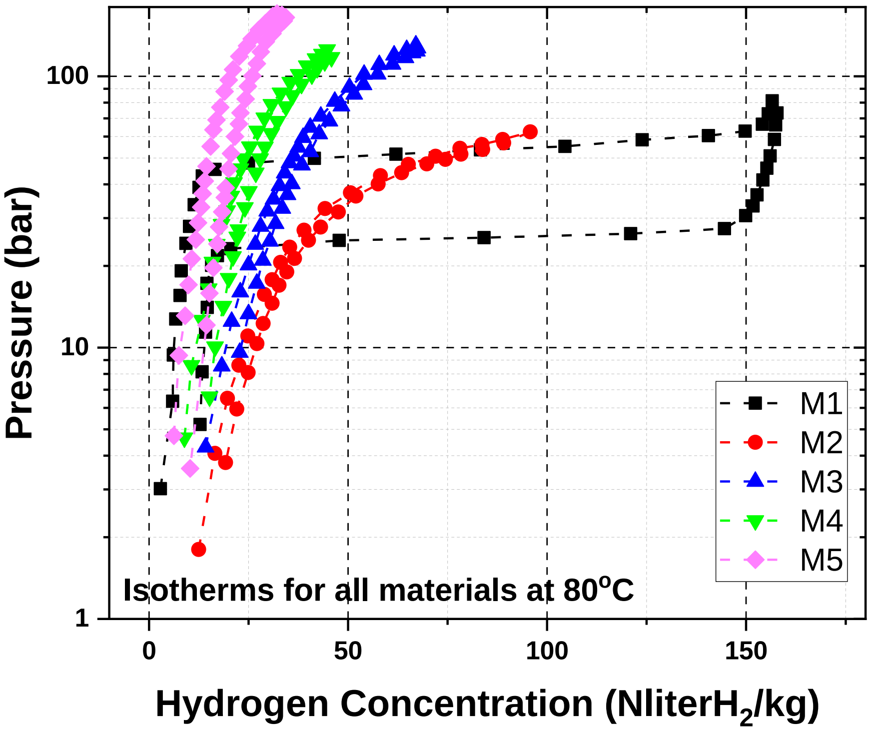

S2. XRD spectra before and after the Hydrogenation process for the sample M1 (S2a) and Rietveld refinement for the Sample M1 before the hydrogenation (S2b)

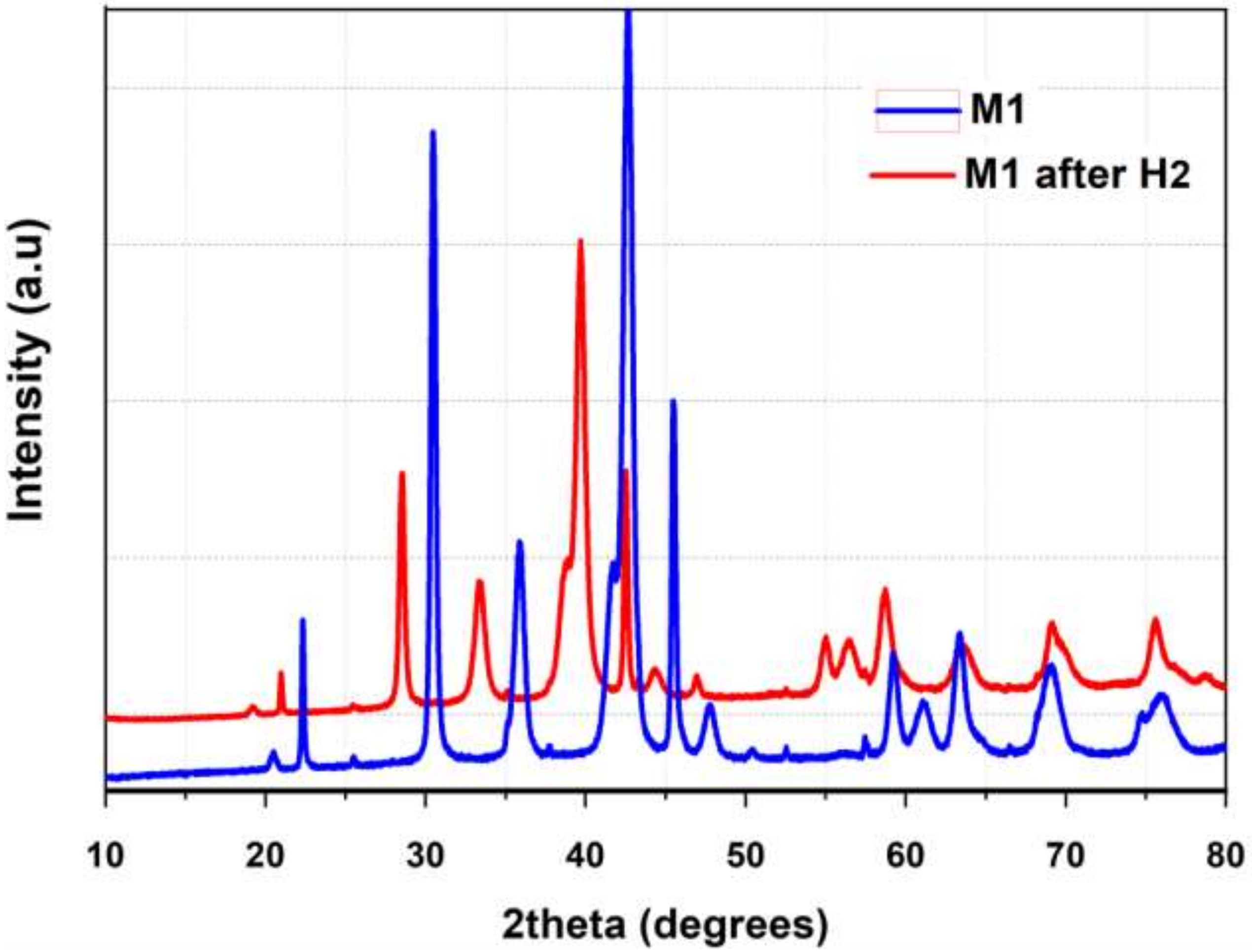

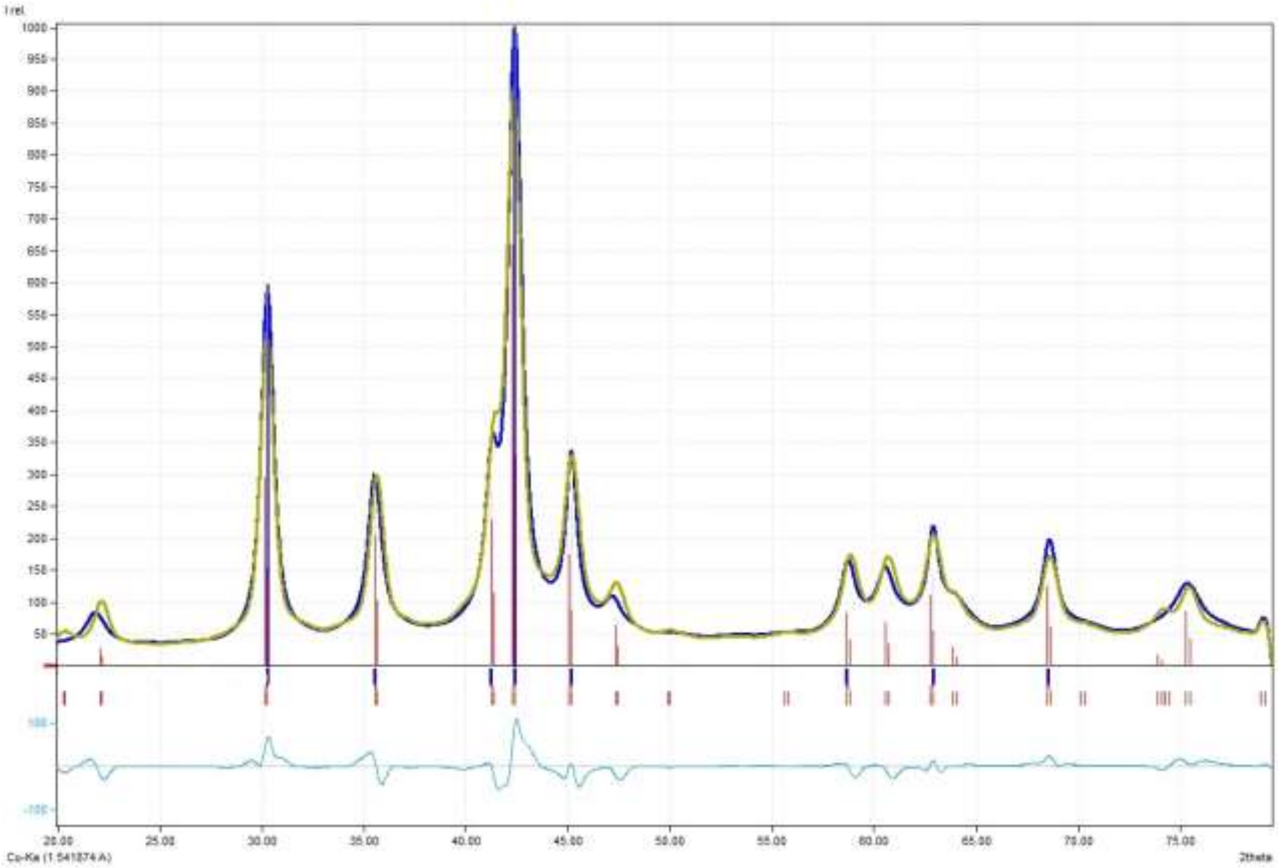
I rel.
1000
950
900
850
800
750
700
650
600
550
500
450
400
350
300
250
200
150
100
50
100
-100
20.00
25.00
30.00
35.00
40.00
45.00
50.00
55.00
60.00
65.00
70.00
75.00
Co-Ka (1.541874 A)
2theta